Materials Science and Engineering R 63 (2009) 81–99

Contents lists available at ScienceDirect

Materials Science and Engineering R

journal homepage: www.elsevier.com/locate/mser

Controlled electron injection and transport at materials interfaces in dye sensitized solar cells

V. Thavasi [a,*], V. Renugopalakrishnan [b,c], R. Jose [a], S. Ramakrishna [a]

[a] NUS Nanoscience and Nanotechnology Initiative (NUSNNI), National University of Singapore, Singapore 117576, Singapore
[b] Children's Hospital, Harvard Medical School, Boston, MA 02115, USA
[c] Department of Chemistry and Chemical Biology, Northeastern University, Boston, MA 02115, USA

ARTICLE INFO

Article history:
Available online 31 October 2008

Keywords:
Nanorods
Nanofibers
Nanowires
Excitonic solar cells
Metal oxides
Electrolytes

ABSTRACT

Dye-sensitized solar cells (DSSCs) generate excitons (bound electron-hole pairs) upon absorption of photon from the sunlight and undergo dissociation at the donor/acceptor materials interface to create free electrons and holes. Major challenges in DSSCs until now have been to achieve maximum exciton generation followed by dissociation, electrons injection and transportation with minimum recombination, which are controlled by the dye/metal oxide, dye/electrolyte, and metal oxide/electrolyte interfaces.

Researchers have been focusing on improving these materials interfaces in DSSCs by using novel materials (doped metal oxides, wider spectral range dyes, and low viscous gel, ionic electrolytes and low molecular weight organic hole conductors), and introducing new semiconductor morphologies (nanofibers, rods, wires, core–shell). With the current effort by researchers, TiO_2/Ruthenium complex (N3 dye)-based liquid state DSSC have reached an efficiency of 11%, whereas TiO_2/Ruthenium complex (N719 dye)/Solid electrolyte-based solid state DSSC have achieved an efficiency of ~4%. As numerous materials have been the focal point in DSSCs, it is necessary to have an overall understanding on the materials interfaces and their influence on the performance of the solar cell. This review focuses on the metal oxides and metal oxide/dye interface that control the electron injection and transport for improving the efficiency of DSSCs.

Contents

1. Introduction . . . 82
2. Dye/metal oxide interface . . . 83
   2.1. Influence of dyes on electron injection . . . 84
   2.2. Effect of dye aggregation . . . 85
3. Role of metal oxide on the performance of metal oxide/dye interface . . . 86
   3.1. Effect of electronic structure of metal oxides . . . 87
   3.2. Effect of chemical stability of metal oxides . . . 90
4. Effect of solvent environment . . . 90
5. Effect of core–shell nanostructure . . . 91

* Corresponding author at: NUS Nanoscience and Nanotechnology Initiative (NUSNNI), National University of Singapore, Faculty of Engineering, Block E3, #05-11, 2 Engineering Drive 3, Singapore 117576, Singapore. Tel.: +65 6516 6593; fax: +65 6872 5563.
E-mail addresses: nnitv@nus.edu.sg (V. Thavasi), seeram@nus.edu.sg (S. Ramakrishna).

Abbreviations: N3 dye, cis-di(thiocyanato)-bis(2,2′-bipyridyl-4,4′-dicarboxylic acid)-ruthenium(II); N719 dye, cis-di(thiocyanato)-bis(2,2′-bipyridyl-4-carboxylate-4′-carboxylic acid)-ruthenium(II); N712 dye, $(Bu_4N)_4[Ru(dcbpy)_2(NCS)_2]$; Black dye, $(C_4H_9)_4N]_3[Ru(Htcterpy)(NCS)_3]$ (tcterpy = 4,4′,4′-tricarboxy-2,2′,2′-terpyridine); Z907 dye, cis-di(thiocyanato)-(2,2′-bipyridyl-4,4′-dicarboxylic acid)(4,4′-dinonyl-2,2′-bipyridyl)-ruthenium(II); Ru, ruthenium; SnO_2, tin oxide; ZnO, zinc oxide; TiO_2, titanium oxide; Nb_2O_5, niobium oxide; In_2O_3, indium oxide; $SrTiO_3$, strontium titanate; ZrO_2, zirconium oxide; MgO, magnesium oxide; Al_2O_3, aluminum oxide; SiO_2, silicon di oxide; FTO, fluorine doped tin oxide; IPCE, incident photon conversion efficiency; η, solar-electric energy conversion efficiency; DMSO, dimethyl sulfoxide; AcN, acetonitrile; EtOH, ethanol; Ace, acetone.

0927-796X/$ – see front matter © 2008 Elsevier B.V. All rights reserved.
doi:10.1016/j.mser.2008.09.001

6. Controlled electron transport by materials used in DSSCs. . . . 92
6.1. Effect of 1D nanostructures for controlled electron transport . . . 92
6.2. Effect of hybrid nanostructure . . . 94
6.3. Effect of nanodimensions . . . 95
7. Conclusion and future directions . . . 97
Acknowledgements . . . 97
References . . . 97

1. Introduction

Today, the most successful photovoltaic devices are fabricated using semiconductor materials such as silicon (Si) [1]. In recent years, several alternatives to Si-based solar cells have become available and considerable research is ongoing towards substantially reducing the cost of electricity generation. Dye-sensitized solar cells (DSSCs) [2–4] are attractive alternative as they can be inexpensive, light weight, portable and flexible.

DSSC possesses three major components: (i) dye sensitizer in order to harvest solar energy and generate excitons [5,6], (ii) nanostructured metal oxide material to transport electrons efficiently [7–9], and (iii) redox electrolyte or hole transporting material, to support the performance of dye and metal oxide [10,11]. The schematic diagram of DSSC is presented in Fig. 1.

The basic principle of DSSC is the photoexcitation of dye resulting in electron injection into the conduction band of the metal oxide (MO), hole injection into the electrolyte, and gets reduced as shown below:

$$Dye^{\oplus\ominus} + MO \underset{\text{electron injection}}{\longrightarrow} Dye^{+} + MO^{-}$$

Redox species, usually comprises of iodide/triiodide redox couple [12], in the electrolyte transport the holes from the oxidized dye to the counter electrode. In the absence of redox species, the injected electrons from excited state of dye undergo recombination with oxidized dye, instead of iodine.

$$Dye^{+} + MO^{-} \underset{\text{recombination with dye}}{\longrightarrow} Dye + MO$$

The redox electrolyte prevents the reduced dye recapturing the injected electron by donating its own electron and thus regenerates the reduced dye.

$$Dye^{+} + 2I^{-} \underset{\text{dye regeneration}}{\longrightarrow} Dye + I_2{}^{-}$$

The oxidized iodide is then regenerated by the triiodide at the counter electrode, with the electrical circuit being completed via electron migration through the external load.

$$I_2{}^{-} + 2e^{-} \underset{\text{iodide regeneration}}{\longrightarrow} 2I^{-}$$

Back electron transfer from metal oxide into the electrolyte is however the primary and predominant recombination pathway in DSSCs, which lower the conversion efficiency.

$$I_2{}^{-} + MO^{-} \underset{\text{recombination with electrolyte}}{\longrightarrow} 2I^{-} + MO$$

The oxidized dye must be regenerated by the redox couple at the speed of *ns* to kinetically compete with the metal oxide electrons for subsequent electron injection as well as to prevent the recombination, which depends on the energetics of metal oxide/dye/electrolyte interface. Interface is the region formed when two phases (systems) are in contact through which the intensive properties of one phase transfer to the other. Energetic interface is the region produced when layering or interpenetrating of two or more materials of different valence and conduction bands or with dissimilar molecular energy levels, *i.e.* highest occupied molecular orbital (HOMO) and lowest unoccupied molecular orbital (LUMO).

Dye/metal oxide interface energetics is created by matching the LUMO level of the dye with (or just above) the conduction band (E_{CB}) of metal oxide. The dye/electrolyte interface is created such that the HOMO level of the electrolyte lies close to the HOMO level of the dye for the fast electron transfer, *i.e.* the ground-state oxidation potential of dye must be sufficiently positive to oxidize the redox couple. The mass transfer rate of the redox species ($I^{-}/I_2{}^{-}$) has to be superior, failing which results in higher electron-transfer resistance and lower conversion efficiency [13]. The ion mobility in the electrolyte has been improved by adding additives: polymers [14–16], inorganic fillers [17–20] and plasticizers [20,21]. Lithium inclusion in electrolyte has been commonly used

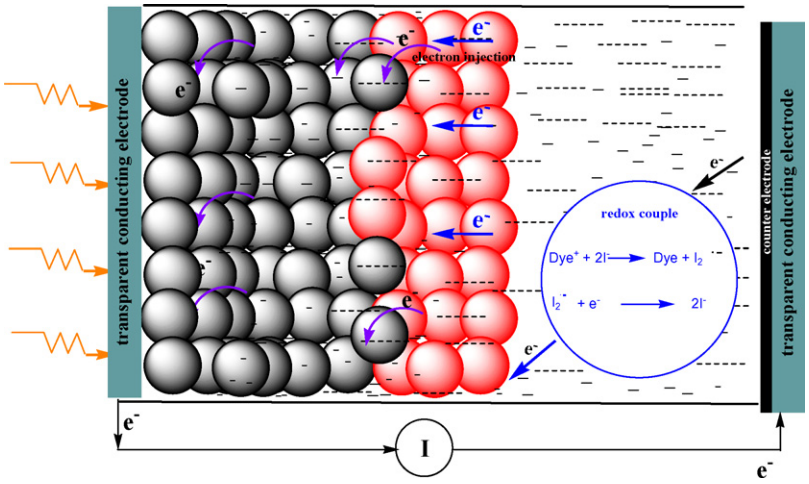

Fig. 1. Schematic diagram of dye sensitized solar cells. Mesoporous metal oxide nanoparticles as photoanode with adsorbed dye sensitizer (red color). Upon photoexcitation, electron is injected into the conduction band of the anode. The anode is percolated with an electrolyte whose redox potential supports for the separation of bound electron-hole pair at the metal oxide and photoexcited dye. (For interpretation of the references to color in this figure legend, the reader is referred to the web version of the article.)

in DSSCs, where Li^+ adsorbs onto the metal oxide surface and increases the charge injection efficiency of dye by shifting the conduction band edge to more positive potentials [22,23]. Researchers have investigated using imidazolium cations in the electrolyte and noticed that the imidazolium cations adsorbs on the metal oxide surface and align the anion species due to electrostatic interaction, and thereby facilitates electron transport [24]. By improving the ionic transport the electron injection efficiency of dye can be enhanced; however, the control of ion composition (and concentration) should be optimal for the higher performance of DSSCs.

The recombination could be minimized if: (i) the rate constant of electron injection from the excited dye into the conduction band of metal oxide should be as small as possible, which depends strongly on the energetics of the metal oxide/dye/electrolyte interface. Much of the current research in DSSC on global has been devoted to the synthesis of dye sensitizers and experiment them on various metal oxides. The primary step to realize the maximum charge injection into metal oxide is to dissociate the bound electron-hole pairs (Frenkel excitons) generated upon photoexcitation of dye [25], which depends on the energetics of dye/metal oxide interface. The dye/metal oxide interface is therefore one of the key issues to be addressed for obtaining higher energy conversion and retaining stability in the photoelectrochemical environment. Therefore, for being significant in DSSC, the metal oxide/dye interface has been emphasized in this review. (ii) Following electron injection into the conduction band of metal oxide by photoexcited dye, electron collection at the collecting electrode requires the transport of electrons in the nanoparticles film to be faster before it undergoes recombination (back transfer), which depends on the nature and nanomorphology of metal oxide. In the nanoparticle film of 10 μm thick, an electron visits approximately 10^6 nanoparticles [26] on an average during transport before reaching the collecting electrode and plausible that such particles morphology acts as a potential recombination site. This review foresees the possibility of using one-dimensional (1D) nanomorphology by which such transport can be minimized by achieving unidirectional transport.

The performance of each interface is crucial and have been designated using the parameters: open-circuit voltage V_{OC}, fill factor *FF*, and short circuit current density J_{SC}, and expressed as efficiency (η) using the equation:

$$\eta = \frac{V_{OC} I_{SC} FF}{P_{in}} \quad \text{and} \quad FF = \frac{I_{max} V_{max}}{I_{SC} V_{OC}}$$

whereas V_{OC}, is the maximum voltage obtained at zero current; I_{SC}, the short circuit current is the maximum current obtained under less resistance (short circuit) conditions and P_{in} is the solar radiation intensity. I_{max} and V_{max} are the maximum current and maximum voltage, respectively. J_{SC} (mA/cm^2) depends on the charge injection and transport. To achieve larger J_{SC}, the transport of electrons must be faster than the reaction with molecules in the electrolyte. Hence, the J_{SC} depends on the performance of oxide/dye/electrolyte interface. *FF* is attributed to functioning of the metal oxide/electrolyte interface. The higher the recombination of conduction band electrons with the electrolyte, the lower will be the *FF*. The electron injection into the conduction band of metal oxide results a dramatic increase in electron density, raising the Fermi level towards the conduction-band edge. This shift of the Fermi level of metal oxide under irradiation increases the free energy of injected electrons and is responsible for the generation of the photovoltage in the external circuit. The V_{OC} is related to the energy difference between the Fermi level of the metal oxide and the Nernst potential of the redox couple in the electrolyte. The V_{OC} is influenced by the electronegativity (electron affinity) of metal oxide, and ionization potential of dye [27,28]. Raising the energy level of the metal oxide conduction band should reduce the recombination losses, and result in high open circuit voltage. The suppression of dark current at the metal oxide/electrolyte interface will increase the V_{OC}.

The maximum achievable theoretical efficiency (η) of the conversion of solar energy–electrical energy has been estimated to be 31% for DSSC [29], however, the highest demonstrated efficiency so far has been only 11% [30]. Maximum charge injection and minimum recombination are the key to achieve higher efficiency. Research has been focused on designing DSSC with various possible materials and their combination (Fig. 2). Control of electron injection and transport at the materials interfaces are central to the design of DSSCs. This review discusses on the materials interfaces that influence efficient electron injection and transportation, especially on three core elements (i) metal oxide, (ii) dye sensitizer, and (iii) metal oxide/dye/electrolyte interface, which are primary determinants in the overall performance of DSSCs.

2. Dye/metal oxide interface

The dye/metal oxide interface is to be designed such that the oxidation potential of excited dye (LUMO) is sufficiently negative to achieve efficient electron injection into the conduction band of metal oxide. Upon photon absorption, the dye molecule (sensitizer) reaches its excited energy state (LUMO) and generates excitons, which diffuse into the dye/metal oxide interface. There will be built-in energy gradient ΔE exists at the metal oxide/dye interface due to the energy difference between LUMO state of excited dye and conduction band of metal oxide (E_{CB}). The electrons in the tightly bound excitons are so attracted by energy gradient, and when this gradient exceeds the binding energy (E_{ex}) of bound excitons, the exciton dissociation occurs:

$$\text{Dye} \xrightarrow[\text{excitation}]{h\nu} \text{Dye}^{\oplus\ominus} \xrightarrow[\text{exciton dissociation}]{\Delta E >> E_{ex}} \text{Dye}^{\oplus\ominus}$$

As the energy level of freed electrons is equivalent to the conduction state of metal oxide, E_{CB}, the electrons are injected into metal oxide, which is also called as forward electron transfer (Fig. 3). LUMO of the excited dye therefore should be in-line with the lower limit of the conduction band of metal oxide to facilitate the effective electron injection into the metal oxide [2,31].

The amount of the sensitizer molecules available for light harvesting and charge injection are important upon adsorbing dye onto the metal oxide. Dye molecules are to be oriented on the surface of metal oxide with attachment functionalities of the molecule. Orientation reduces the covering area per adsorbed molecule, providing a more compact and packed arrangement of the dye molecules, which allow for more adsorption dye of molecules. The rate constant for the migration of the excited energy would depend on the relative orientation of the donor and acceptor moieties. However, this is no longer possible if the dye is adsorbed as aggregates. Problem of poor electron transfer to the metal oxide conduction band would be arisen if dyes are aggregated that results in an unsuitable energetic position of the LUMO level. Lower current density could be resulted by poor injection efficiency, due to unfavourable binding of dye onto the metal oxide surface. The orientation of the molecule on the metal oxide surface is characterized by the anchoring group present in the dye [32]. Anchoring groups of dye to the semiconductor surface is the most decisive factor help in bringing the relative orientation of energy level of donor and acceptor during the attachment on the metal oxide and increase injection efficiency. The electronic coupling strengths differ depending on the relative position of the LUMO of the dye and its anchoring group [33]. The closer distance between

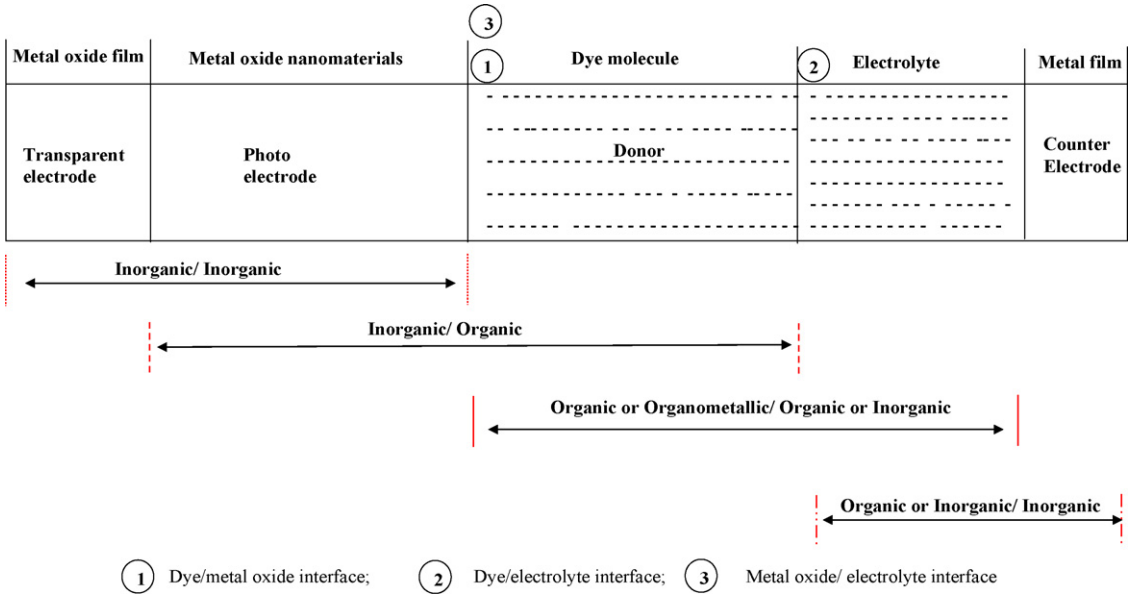

Fig. 2. Combination of materials and interfaces involved in DSSCs.

the anchoring group and the nearest LUMO is preferred for maximum and efficient electron injection. It is to be mentioned that the unique properties of dye sensitizer as well as metal oxide affect electron injection when combined for forming dye/metal oxide interface [34]. In this part of review, the structural influence of dye sensitizers, *i.e.* the effect of binding mode and number of anchoring groups while forming dye/metal oxide interface on the electron injection efficiency are focused, whereas on the metal oxides aspect, the chemical property and electronic structure are discussed.

2.1. Influence of dyes on electron injection

Dye sensitizer bound via its electronically favorable binding mode is preferable for enhancing electron injection efficiency. Metal oxide/dye interface in DSSCs is created by firmly grafting the dye with its anchoring group such as carboxylic acid or phosphonic acid coordinated onto the metal oxide. Dyes anchored with phosphonic acid have demonstrated better long-term stability against moisture in the environment compared to carboxylic acid anchors which usually degrades upon absorption of moisture [35]. However, the rate of electron injection from the dye via the carboxylic group has been found almost twice when compared to binding via the phosphonic anchor group [36]. Thus, larger photocurrents can be obtained for dyes that link with its carboxylic acids [37]. Electron injection from higher excited states is most likely is vibrational in origin, *i.e.* hot electrons from the dye into the metal oxide and hence there is a mandatory requirement for proximal contact between the dye and metal oxide. This suggests that the dye–metal oxide distance should be shorter and therefore

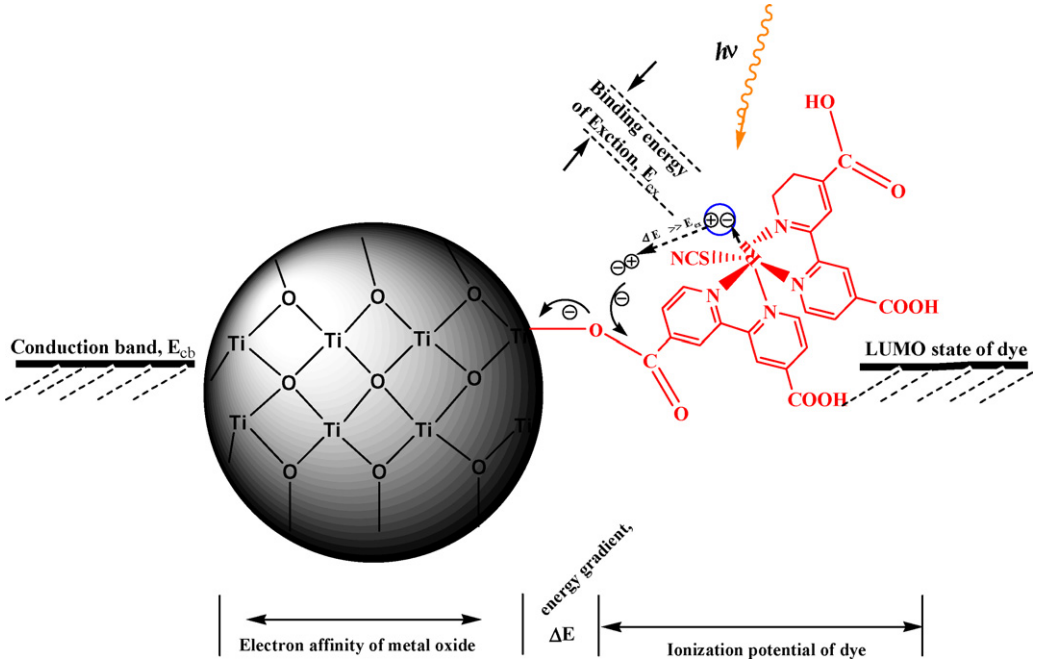

Fig. 3. Schematic illustration of exciton dissociation at the metal oxide (TiO2)/dye interface and electron injection into metal oxide.

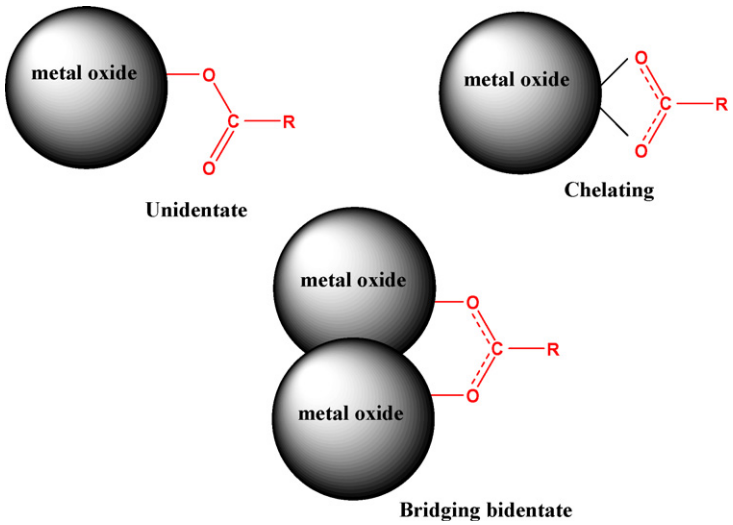

Fig. 4. Possible binding modes of carboxylic acid group of dye onto metal oxides surface.

mode of linking of dye on metal oxide needs more attention. Previous researchers have found that the dye links onto TiO_2 surface through bridging bidentate coordination mode (Fig. 4) is more stable and preferable [38–40] because the bidentate binding is shorter and hence increase in the rate of electron injection could be expected.

For carboxyl group binding to occur, there should be an electronic coupling between the cationic metal and oxygen atom of the carboxylic acid which promote electron transfer upon photoexcitation. The nature of linking of carboxyl group onto the metal oxide also plays a role in enhancing electron injection. The carboxyl groups can either form ester-like linkages (C═O) or carboxylate linkages (C–O–O–) with metal oxide, via titanium atom in the case of TiO_2. Carboxyl binding (C–O–O–) results in a decrease of electron density of the ligand, leading to the lower energy shift in band. Nazeeruddin et al. [40] have observed higher energy conversion efficiency for N3/TiO_2 interface formed by anchoring N3 via two of their carboxylate groups. Due to numerous carboxyl groups present in N3 dye, carboxylic acid anchoring by unidentate linking may not be stable enough, and it tends to transform into bridging or bidendate because of large rotational freedom of dye molecule. Black dye that is comparable with the performance of N3 dye has also been observed to anchor via carboxylate link with TiO_2 rather than ester link [41]. Likewise, N719 dye which contains two carboxylic groups has also been ascertained to bind via two carboxylates. While realizing carboxylate mode is important for effective electron injection and phosphonate group for stability, it is to be noted that both stability and performance are crucial issues in DSSC and therefore have to be compensated. The ester linkage may be preferred as it is stable (covalent like) on metal oxide and because of its stronger electron withdrawing nature, enhanced electron injection could be obtained. Morakoshi et al. [42] have induced ester linkage (C═O) in N3 dye by reflux treatment and compared its conversion performance with N3 linked via carboxylate (COO–) mode to TiO_2. They have found that the ester linkage of N3 dye onto TiO_2 shows higher conversion efficiency than that of carboxylate-link mode. Recent study has evidenced that rhodamine B sensitizer anchored on TiO_2 via ester linkage (C═O) delivers the photocurrent of 2 orders of magnitude greater than that of dye linked with its amide mode [41]. The ester-like linkage from the carboxylic acid group of dye may be favorable for efficient electron injection.

2.2. Effect of dye aggregation

Dyes manifest poor electron injection if it is adsorbed on a metal oxide in unfavorable adsorption geometry [43]. N3 dye has two bipyridine ligands and four carboxyl groups in its structure and adsorption may occur via several modes viz. protonation of one or more of all the four carboxyl groups [40], which results in difference in their energy levels that in turn lead to differences in their electron injection efficiency. For example, the fully protonated N3 dye, while possessing an excellent light-harvesting capability, shows poor electron injection efficiency due to the misalignment of the dye on TiO_2 (Fig. 5) [31]. The LUMO of fully deprotonated N3 dye lies well above the TiO_2 conduction band (~3.2 eV), and therefore excited state relaxation to the bottom of the conduction band of TiO_2 may suffer from some energy loss [44]. The di- and mono-protonated forms of N3 dyes provide perfect alignment of their excited states with respect to the TiO_2 conduction band and therefore manifest light-harvesting property at such orientation. Nazeerudin et al. [40] have obtained the energy conversion efficiency of 7.4% for N3 dye with four-protonated groups, but 9.3% for mono-protonated N3 dye. The larger number of protons carried by the sensitizer influences the energetics of the conduction band of metal oxide, decreases the driving force between the dye and the redox couple, and thereby reduce V_{OC} of DSSCs. Therefore, the degree of dye protonation has profound influence on the energy conversion performance.

The number of protons plays a significant role in the electron injection efficiency. Nazeerudin et al. [40] have observed that mono-protonated form of N3 dye exhibits higher conversion efficiency compared to the four, two, and zero proton sensitizers after examining N3/TiO_2, N719/TiO_2, and N712/TiO_2-based DSSCs. They have observed that the mono-protonated N3-based DSSC delivers the J_{SC} of 19 mA/cm^2, whereas di-protonated N712 and zero-protonated N719 showing 13 and 17 mA/cm^2, respectively. It clearly emphasizes that the degree of protonation of the sensitizer influences both J_{SC} and V_{OC} and therefore has to be optimized for higher conversion efficiency of DSSC. Nazeeruddin et al. [40] has proposed that the one proton dye is the optimum for high-power conversion efficiency of the DSSCs. Other researchers have achieved 100% efficient electron injection from mono protonated N3 dye into TiO_2 [45]. Likewise, a conversion efficiency of 11.2% has been achieved for the mono-protonated N719/TiO_2 interfaced

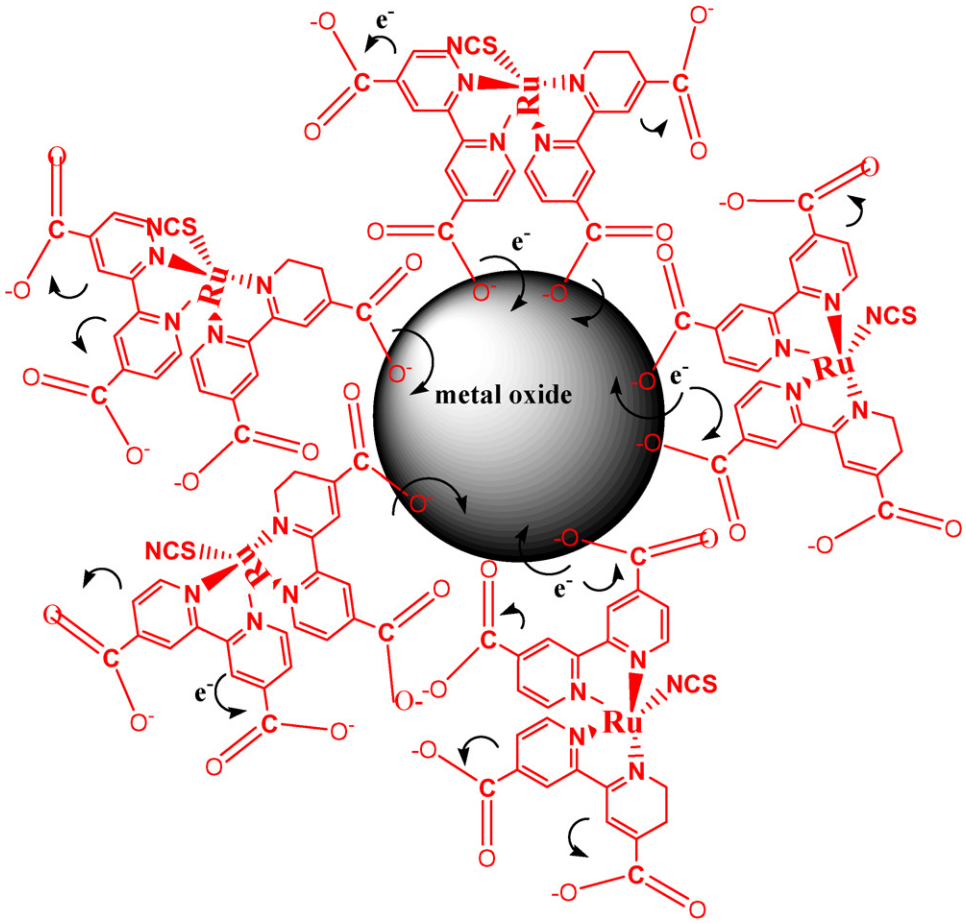

Fig. 5. Inefficient electron injection into metal oxide arises from misalignment and higher degree of protonation in N3 dye.

solar cell under AM 1.5 with 17.73 mA/cm^2 J_{SC} as 0.846 V, V_{OC} as 0.75 for 0.158 cm^2 cell [30].

The electron injection efficiency can also be influenced by the aggregation of dye molecules on the metal oxide surface. Less aggregated or zero-aggregated dye anchoring onto the metal oxide should be desirable for faster electron injection. Dyes show slower electron injection or self-quenching if it undergoes aggregation, which can be encountered either before or during processing of dye for adsorption onto metal oxide. Processing methods such as sonication or stirring that are used to dissolve the dye powder in solvent could cause dye aggregation upon excessive treatment. Rapid method of interfacing dye with metal oxide form dye aggregates that are less efficient in both electron injection and dye regeneration by iodide [46]. This kind of aggregation can be minimized quite easily by adopting precise engineering control on the process. However, another kind of aggregation of dye occurs during anchoring via intermolecular hydrogen bonding [43] and hence caution must be observed in the proper selection of dye for the respective metal oxides. For instance, black dye (Fig. 6) has been reported to form aggregates on the metal oxide surface due to the long alkyl chain that undergoes hydrogen bonding during anchoring and thereby affects the electron injection performance. Presence of numerous carboxyl groups also facilitates aggregation. Larger number of the carboxyl groups in the dye sensitizer increases the electron-transfer efficiency due to their better anchoring to the surface [47], however, numerous carboxyl groups could offer steric hindrance which results in an uncoordinated binding onto the surface. Lesser the number of COOH groups, lower the possibility that it undergoes H bonding, and causes aggregation. Z907 dye has lesser number of COOH groups in its structure which allows for well organized self-assembly onto the metal oxide surface. Hence, no self-quenching can be expected in Z907 interfaced metal oxide (Fig. 7). The creation of energetic metal oxide interface with such dyes and with wide spectral coverage should lead to higher energy conversion efficiency and stable DSSC. Even so, the dyes with one COOH group also cause slow electron injection. For example, cyanine-based organic dyes L3 and L4 (Fig. 8) interface with TiO_2 have caused poor injection efficiency, most likely originating from unfavorable binding or orientation of these dyes onto the TiO_2 surface [48]. It is important to stress that the factors such as orientation, nature of binding, and structure of the dyes influence the electron injection efficiency and thereby enhance the overall performance of DSSC.

3. Role of metal oxide on the performance of metal oxide/dye interface

A schematic of energy level diagram describing the charge transfer processes involved in DSSC is shown in Fig. 9. Electron injection from dye sensitizer usually occurs in ultrafast time scale and followed by a slower time scale, which have been denoted as fast and slow components, respectively, using biphasic (two-state) model [49,50]. The fast and slow components are attributed to injection from unthermalized and relaxed excited states of dye, respectively (Fig. 9). It is to be noted that the rate of electron injection is significantly contributed from unthermalized excited state (*i.e.* fast component) and plays major role in the electron

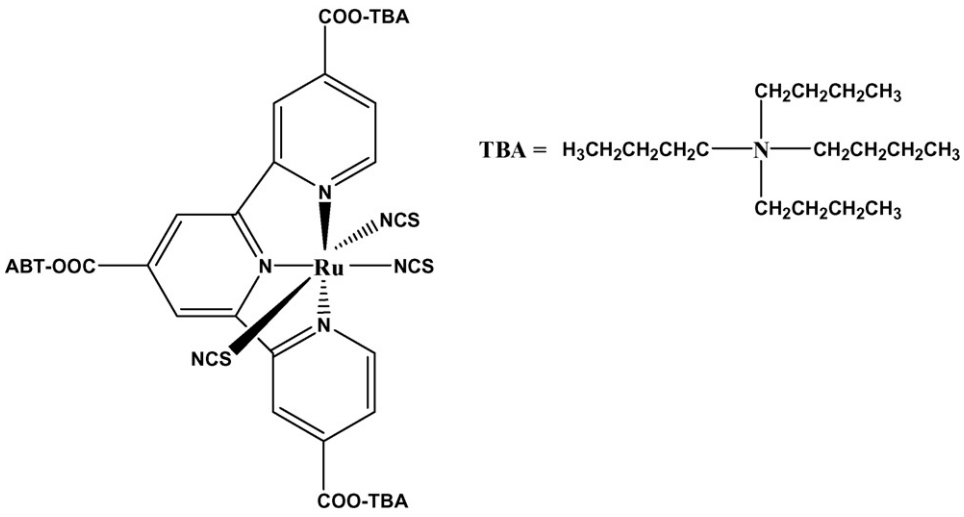

Fig. 6. Structure of black dye.

injection efficiency. For N3/TiO_2 system, the rapid electron injection from N3 into TiO_2 has occurred within 250 *fs* [44], whereas for N3/ZnO system, the injection time scales for fast component has been estimated to be 1.5 *ps* [51]. For N3/SnO_2 system, the electron injection speed have been found even slower, *i.e.* 5–10 *ps* [52–54].

For the invariant LUMO value of N3 dye, but for different metal oxides it has been found that the injection speed differs, suggesting that metal oxide energetics could play a role. Energetically, the conduction band edge value (E_{CB}) and band gap are similar for TiO_2 and ZnO [55–57]. For the same LUMO level of N3 and with similar energy values of TiO_2 and ZnO, it is reasonable to expect the similar rate of injection. Nevertheless, the electron injection has been found faster in the case of N3/TiO_2 that that of N3/ZnO. Likewise, on the basis of energetics, SnO_2 is expected to provide better electron injection rate compared to TiO_2 since its E_{CB} edge position is 0.5 V lower than that of TiO_2 (see Fig. 9 and Table 1). The rate of electron injection has been however slower than TiO_2. Overall, the injection efficiency for the widely studied metal oxides has been found in the following order: $TiO_2 > Nb_2O_5 > SnO_2 \sim ZnO \sim SnO_2$ [58,59]. The energetic difference in metal oxides is unable to account for the orders of magnitude difference in injection rate. An important aspect that distinguishes metal oxides among each other is the electronic structure, and hence researchers have taken electronic structure of metal oxides into account to explain the difference in injection and performance.

3.1. Effect of electronic structure of metal oxides

According to Marcus theory of interfacial electron transfer, the rate of electron injection under nonadiabatic condition is proportional to the density of accepting states (DOS) in the conduction band of semiconductor. Electronic structure of the conduction band is usually comprised of empty *s*, *p*, *d* and *f* orbitals. The conduction band of SnO_2 is composed primarily of empty *s* (and *p*) orbitals of Sn^{4+}, whereas TiO_2 is composed primarily of empty *d* orbitals of Ti^{4+}. The *d* bands are typically narrower, whereas *sp* bands are broader and having density of states (DOS) an order of magnitude smaller than *d*-type conduction bands. The electron-transfer integrals for the *d*-orbitals of the neighboring metal atoms are smaller than that of the integrals for *s*-orbitals. Therefore, the effective mass (me) of the conductive electron should be larger for *d*-orbital materials. When the effective electron mass is larger, the DOS near the conduction band edge also becomes larger. The electron effective mass in *d*-type conduction bands (5–10 me and 3 me for TiO_2 and Nb_2O_5, respectively) is higher than *i*-type conduction bands (0.3 me for SnO_2 and ZnO). This could be attributed for slower electron injection rate at SnO_2/dye and ZnO/dye interfaces compared to TiO_2/dye interface.

Upon photoexcitiation, the Ru dye complex transfer the electronic charge density first to ligand orbital which is in intimate contact with the conduction band of the TiO_2. For Ti^{4+}, the orbital structure is as follows:

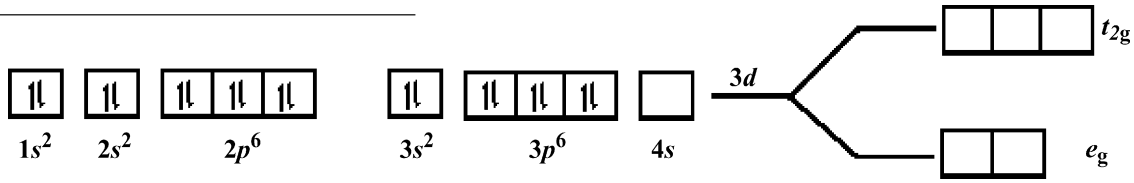

Table 1
Properties of metal oxides that influence the performance of dye/metal oxide interface.

Material	Isoelectric point	Band gap	E_{CB} = 0.0 V versus NHE	Electron affinity	Density of states (effective electron mass)	Electronic structure
Anatase TiO_2	5–6	3.3	0.5 V	3.9 eV	5–10 me	*d* orbitals of Ti^{4+} density of states is higher than others
ZnO	4–9	3.3	Close to TiO_2 ~0.5 V higher than SnO_2	4.5 eV	0.3 me	*s*, *p* orbitals of Zn^{2+}
SnO_2	2.5–4.0	3.5	0.5 V lower than TiO_2	4.8 eV	0.3 me	*s* and *p* orbitals of Sn^{4+}
In_2O_3	7.1	3.6	0.5 V lower than TiO_2	4.45 eV	0.3 me	*s* orbitals of In^{3+}
Nb_2O_5	2.6–4.5	3.4	0.2–0.3 eV higher than TiO_2	2.34 eV	3 me	*d* orbitals of Nb^{5+}

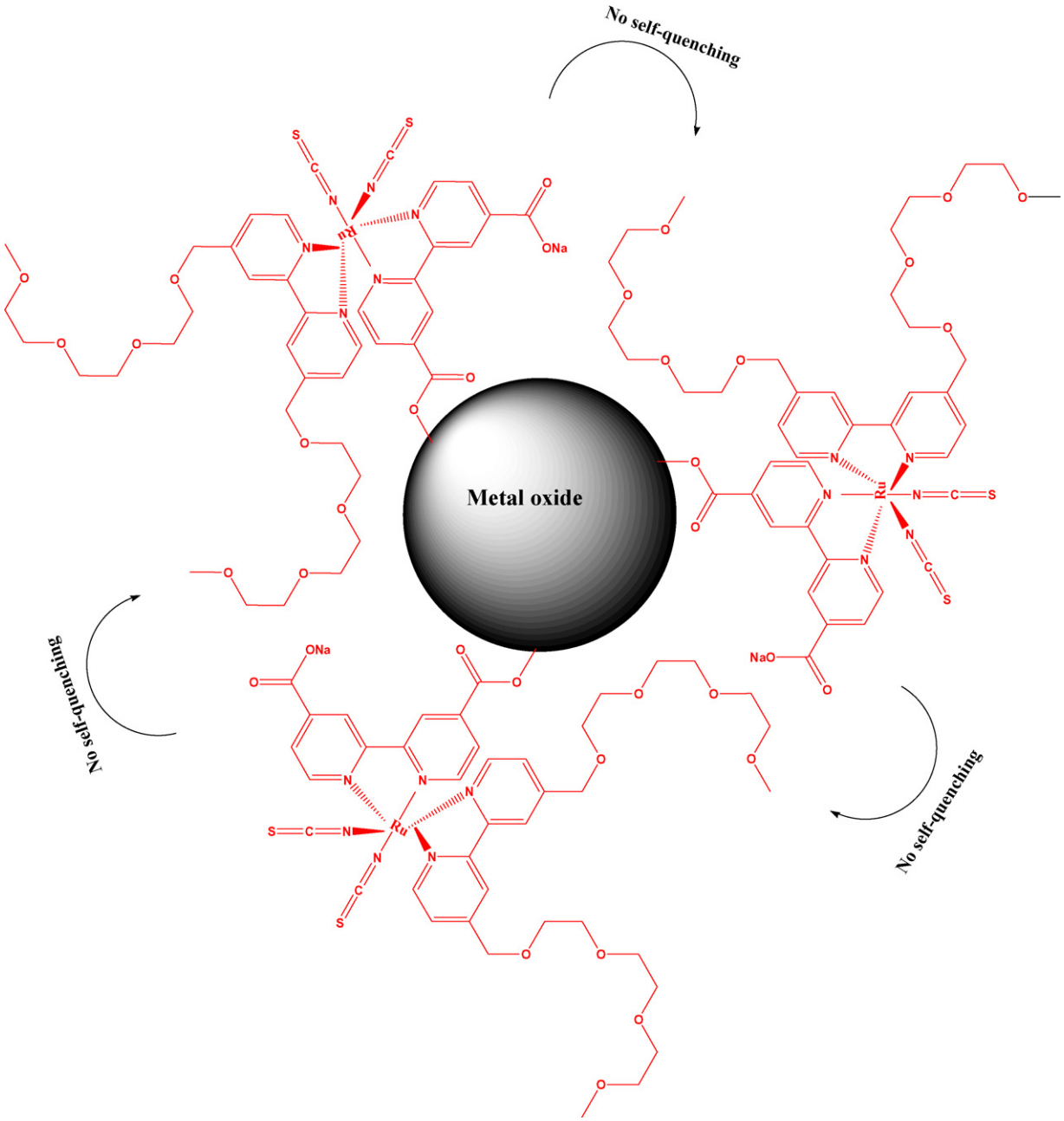

Fig. 7. Well organized self-assembly of Z907 dye onto the metal oxide prevents aggregation and self-quenching.

The 3*d* orbitals of Ti^{4+} are near the conduction band edge of TiO_2. The di-carboxyl bipyridyl ligand in dye molecule exerts back bonding with the Ru complex that actually enhances the acceptor strength of π orbitals of ligand. The electron injection from the ligand goes into the vacant t_{2g} orbital as the excited electron donating ð* orbitals match with the ð symmetry t_{2g} *d* orbitals of Ti^{4+} atoms, and reducing it to Ti^{3+}. Overall, the substantial increase in electron injection occurs from excited dye to TiO_2 [60]. Moreover, this phenomena enable a back bonding reaction, facilitating the formation of a temporary interfacial Ti^{3+}–ligand–Ru^{3+} charge transfer complex. This could allow the longer survival of dye sensitizer molecules on TiO_2 compared to ZnO in an entirely consistent way. The back bonding of metal oxide and Ru complex increases stability while enhancing increased electron injection. Whereas in ZnO/dye system, the beneficial role of back-bonding of bipyridyl ligands with Ru could not be utilized due to the lack of vacant *d*-states in Zn^{2+} (as shown below).

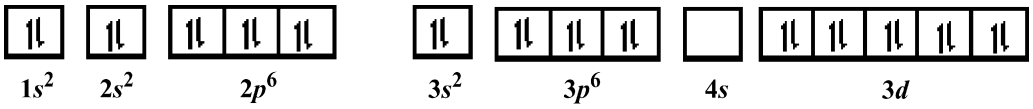

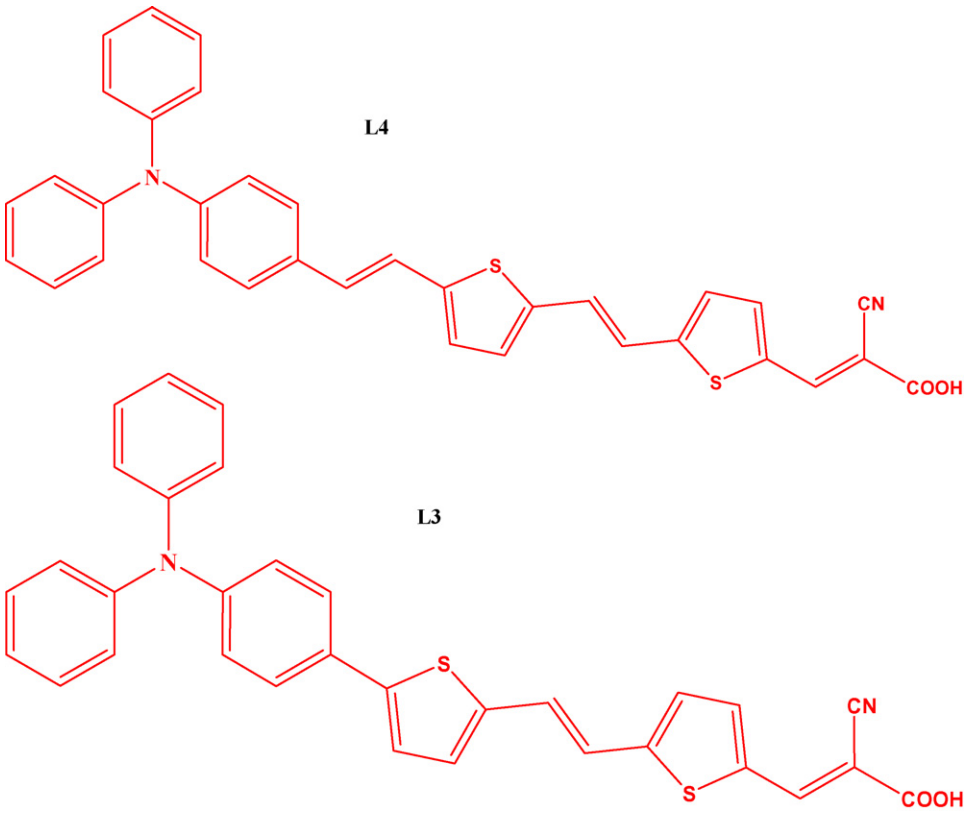

Fig. 8. Cyanine-based organic dyes.

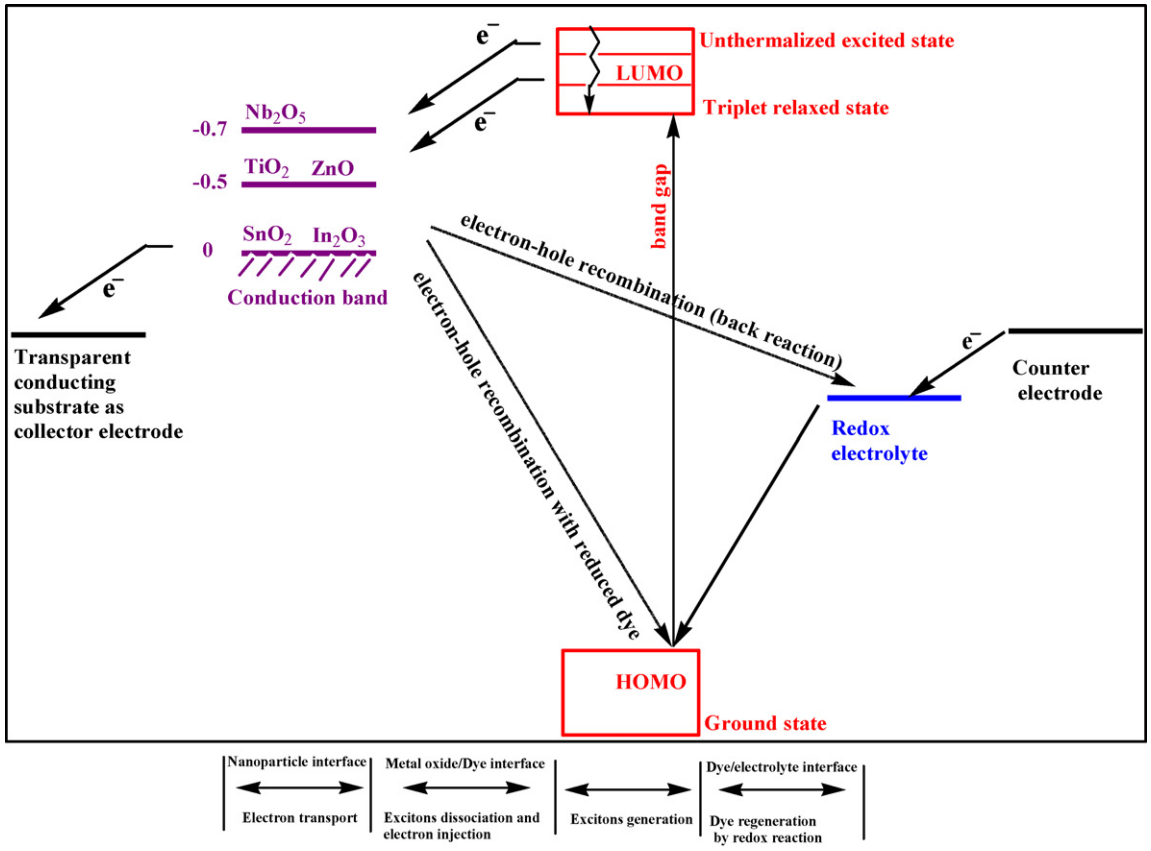

Fig. 9. Energy level diagram for metal oxide/dye/electrolyte interfaces.

Thus replacing Ti by Zn would decrease the stability due to lack of back bonding, and affect the electron-transfer process over the period of time. As the long-term stability of dye (~20 years) is one of the goal of DSSC for industrial feasibility [61], design of such dye/MO interface that enable back bonding of metal oxide and excited dye metal complex may be preferred.

3.2. Effect of chemical stability of metal oxides

It is to be noted that the surface of metal oxides especially ZnO is more prone to be affected by material process conditions during interfacing with dye and electrolyte. Prolonged immersion of ZnO in high concentration of dye leads to more binding of N3 dye, simultaneously allow for the formation of Zn^{2+} aggregates, which deteriorates the surface of ZnO [62]. The formation of dye agglomerates does not take place in the case of TiO_2 but apparent in ZnO. As a result, there should be a reduction in the photocurrent as aggregation makes dye passive for electron injection. Moreover, such dye aggregates block the pores of the ZnO matrix [63], reduce the interpenetrating ability of electrolyte, and substantially decrease the cell efficiency. Formation of dye agglomerates mainly hinges on to the high acidity nature of the carboxylic groups of the dye or pH of electrolytic composition or surface chemical property of material. The isoelectric point (IEP) of material is the pH at which the materials surface carries no net electrical charge. At a pH below the IEP, metal oxide surface carries a net positive charge, and above the pH, the negative charge predominates. IEP is therefore an important parameter by which the difference in injection efficiency at the metal oxide/dye interface could also be arisen because it determines the stability of the dye. Commonly used metal oxides have well defined characteristic IEP values, and are given in Table 1.

The IEP of TiO_2 is about 4–6 and hence DSSC experiment carried at normal conditions, *i.e.* at pH 7 could make the surface more negative. It therefore could facilitate electron injection from the dye more effectively. The IEP of ZnO lies at 9. The agglomeration Zn^{2+} ions could be occurred due to the presence of protons from the acidic carboxylic groups of the dye. Hence, to facilitate more electrons injection, ZnO has to be processed in more basic medium (pH > 9). ZnO-based DSSCs would require alternative sensitizer that does not possess acidic protons in order to suppress the dissolution of zinc ions (Zn^{2+}) and prevent formation of Zn^{2+}/dye aggregates. The dye N719 has lesser number of COOH groups and could exhibit lesser or no agglomeration on ZnO surface than the N3 dye. Recent study has been noticed that N719 dye/ZnO system does not involve in the shift (blue-shift) of absorption spectrum of the N719 dye, evidencing that there is no formation of the Zn^{2+}–N719 dye complex (which actually engages blue-shift) and has also yielded better η of 2.1% for N719/ZnO [63]. Another study has revealed that N719/ZnO interface shows the highest quantum yield for electron injection, *i.e.* 3-fold larger than the N3/ZnO system [64]. As such, N719 may be favorable for interfacing with ZnO. Mercurochrome, an organic dye (Fig. 10) is also preferred for ZnO as it can prevent the formation of aggregates and moreover, cheaper than the Ru-based dyes. A recent study on mercurochrome/ZnO system has unveiled that there is a reduction in recombination rate [65], evidencing that the interpenetration of electrolyte is improved by eliminating the formation of Zn^{2+} aggregates. As a result although mercurochrome can not absorb like N3 dye especially in the light region from 600 to 800 nm, mercurochrome/ZnO system has delivered better η of 2.5% at 99 mW/cm^2 than that of N3/ZnO system (0.4% 119 mW/cm^2). Thus the mercurochrome is a preferred dye over N3 dye to interface with ZnO, emphasizing that suitable combination of dye and semiconductor is mandatory for the construction of high performance DSSCs.

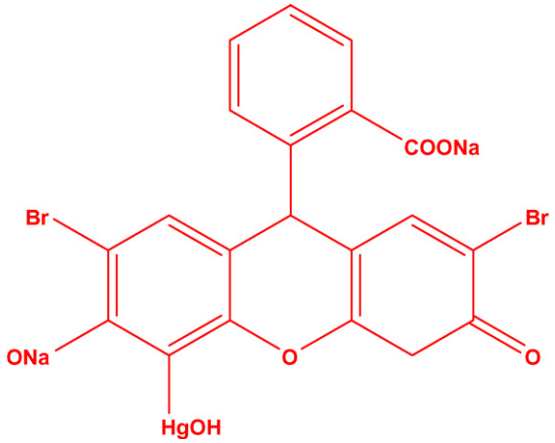

Fig. 10. Structure of mercurochrome dye.

4. Effect of solvent environment

Upon electron injection, the dye gets oxidized and therefore must be regenerated by the redox couple at nanosecond time scale (ns) for subsequent injection as well as to prevent the recombination of metal oxide electrons with the oxidized dye. Therefore the challenge is to obtain optimal dye regeneration efficiency, which depends on the dye/electrolyte interface. While designing dye/electrolyte interface energetics, we need to bear in mind the HOMO energy level of dye lower than the redox couple in the electrolyte [66], one has to make sure that the solvent in the electrolyte solution does not affect the regeneration of dye, and thereby its capacity for electron injection.

For N3/TiO_2 system, the environmental effect may not be as significant as black dye/TiO_2 because the energy gap between the LUMO of the N3 and E_{CB} of TiO_2 is relatively larger. The electron injection dynamics will be sensitive to the environment if the energy gap between the LUMO of the dye and the conduction band (E_{CB}) of metal oxide is smaller. For instance, the energy gap between the LUMO of black dye and the E_{CB} of TiO_2 is relatively small because LUMO of black dye is located just above the conduction band (E_{CB}) of TiO_2 [67] and, therefore electron injection should be sensitive to the environments such as presence of additives and solvent in the electrolyte. The electron injection from dye has been found to be faster in acetonitrile (AcN), a dipolar solvent when compared to polar protic ethanol (EtOH) and polar aprotic DMSO [68]. The rate of electron injection from dye into TiO_2 has been found to be in the following order; AcN > EtOH > DMSO. The difference in the electron injection of dye in the solvent medium could be ascribed to the interactive ability of solvent. Electrolytic solvent molecules may engage through intermolecular interaction with the COOH group of dye molecules and can intercept the dye's electron injection in two possible ways; (i) at excited state and (ii) at the oxidized state. As laid out in Fig. 11a the interaction of acetonitrile with the excited dye is prevented or weakened due to the lower electronegative nature of N atom of acetonitrile. This may allow the excited dye to release (inject) their electrons considerably faster into the metal oxide. This could also allow an additional pathway for electron injection in the acetonitrile medium. Hence faster injection is observed in AcN mediated electrolyte. Higher electronegative nature of O atom in solvents such as ethanol and acetone could exert stronger molecular interaction with the functional group of the dye (Fig. 11b) which will influence the excited-state charge-transfer kinetics and energetics. As a result, the electron injection is restricted, which could lead for the slower electron injection

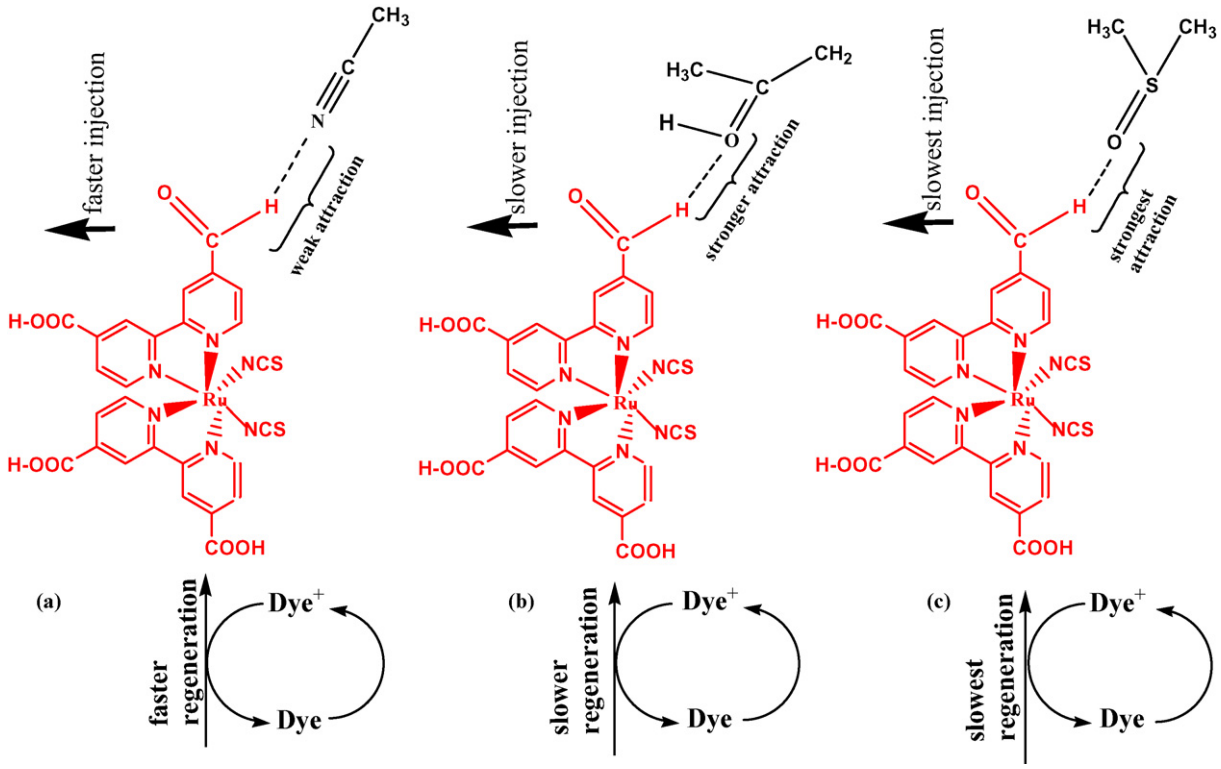

Fig. 11. Effect of electrolyte solvents on the electron injection performance of dye; (a) N3 dye exhibits a weak interaction with acetonitrile, (b) N3 dye forms a stronger interaction with ethanol, (c) N3 dye forms a strongest interaction with DMSO.

kinetics in EtOH. A very strong intermolecular attraction is expected between excited dye and lone pair oxygen atom of DMSO because of the strongest electronegative nature of O atom, that could change the energetics of the excited dye, results in slower injection rate (Fig. 11c). The strong interaction with solvent at the oxidized state of dye change the energetic level, restricting the acceptance of new electrons from the redox couple, which slow down the subsequent injection.

5. Effect of core–shell nanostructure

Control of interfacial electron injection and recombination at the metal oxide/dye/electrolyte interfaces is pivotal for the best performance of DSSCs. Doping at the dye/metal oxide interface has received increased attention among researchers to improve the injection efficiency and suppress the recombination as the interfacial energetics can be controlled by this strategy. Introducing cations as dopant on the surface of photoanode materials (metal oxides) exerts larger dipole moment that changes the interface energetics in an energetically more favorable way for electron transfer [69]. Recombination rate will be diminished because the doped cations could shield electron back flow through metal oxide to the electrolyte. The doping of strontium ions onto the TiO_2 (*i.e.* $SrTiO_3$) has been observed to shift the E_{CB} in the negative direction, *i.e.* from −4.1 to −3.7 eV [70,71]. Conduction shift in the negative direction increases the efficiency of electron-hole separation at the interface and reduces the electron/electrolyte recombination rate and thus increases photocurrent. The reduction in the recombination rate results in larger V_{OC} [69]. Insertion of another metal oxide as shell or interface modifier also controls the back electron transfer, as the shell layer forms a surface energy barrier, which slows down the recombination [69,72–74]. If dethermalization of electron occurs upon travelling in the matrix of the anode material, such electrons can be abstracted by shell material, *i.e.* second metal oxide rather than being back injected into the electrolyte due to its lower E_{CB} nature (Fig. 12).

Roh et al. [75] have observed that the ZnO adsorbed/deposited as shell material on TiO_2 with a thickness of 30 nm at TiO_2/N3 interface reduces electron-hole recombination and reaches an efficiency of 4.51% at 80 mW/cm^2. Presence of Al_2O_3 shell layer on TiO_2 [76] has also been observed to retard the recombination dynamics by passivating surface recombination centers and decreasing the rate of back electron transfer. Al_2O_3-coated SnO_2 has been reported to increase V_{OC}. The presence of MgO as SnO_2/MgO/N719 interface has been observed to deliver a higher photocurrent (J_{SC} of 9.7 mA/cm^2) [77], compared to SnO_2/N719 suggesting that the MgO is involved in the suppression of charge recombination. The performance of shell material depends on their layer thickness at metal oxide/dye interface [78,79]. For example, it has been noticed that ZnO shell layer with larger thickness (>30 nm) leads to leakage of electrons to the electrolyte because of its low electron effective mass, 0.3 me [75]. Similarly, 1 nm thick MgO layer at SnO_2/dye interface and 1 nm thick Al_2O_3 at TiO_2/dye interface have resulted in 4-fold [80,81] and 3-fold [82,83] decrease in the rate of recombination, respectively. Increasing the thickness of Al_2O_3 layer on TiO_2 has resulted in larger decrease in J_{SC}, but not much in *FF* and V_{OC}, indicating that the thickness of shell layer mainly affects the electron transfer. The literature data in Table 2 reveals that larger band gap materials: MgO, Al_2O_3, and SiO_2 as shell layer have resulted in larger J_{SC}, which could be arise from larger enhanced electron injection. Whereas smaller band gap materials such as zirconia (ZrO_2) and $SrTiO_3$ have not significantly improved the photocurrent from TiO_2/dye interface compared to that of larger band gap materials. It has been noticed that the absorption spectrum of MgO-coated TiO_2 is similar to that of neat TiO_2, evidencing that light absorption spectrum of core (photoanode) material is not be affected by the presence of larger

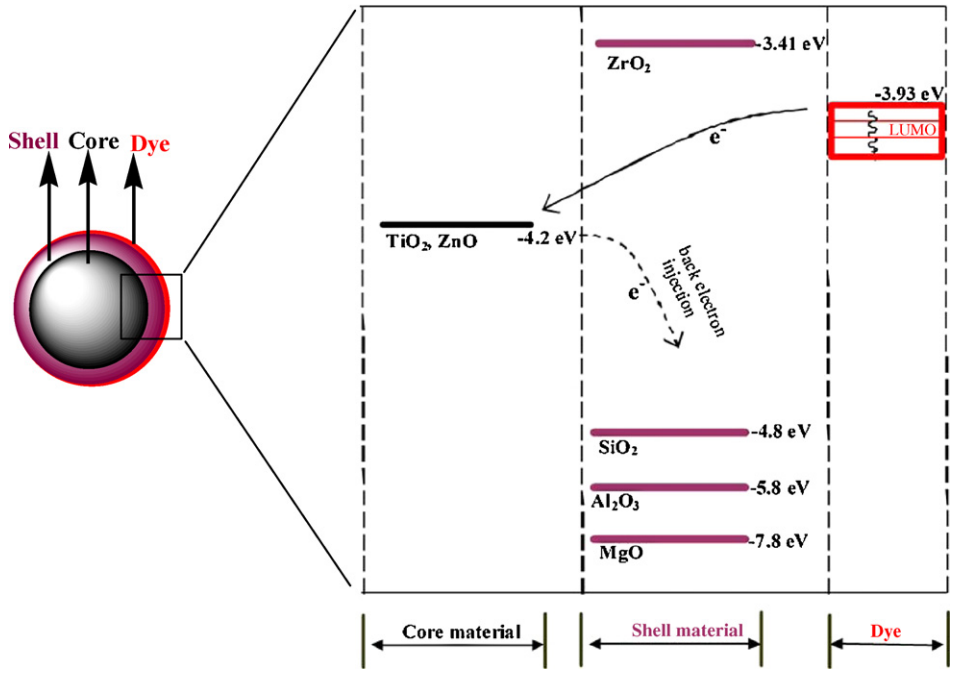

Fig. 12. Energy level diagram for the core–shell metal oxide interface with N3 dye.

band gap shell material. Thus, the surface modification of photoanode electrodes with very thin layer as well as larger band gap shell material improves the photocurrent.

It is reasonable to expect a bond formation between core and shell material because of the process conditions involved in device making: high temperature sintering, and solvent treatment, etc., which could change the electronic property of the core anode materials. For example, the SiO_2 as shell layer on TiO_2 could modify the electronic structure of the Ti atoms by forming Ti–O–Si bonds at the inter-phase boundary of TiO_2–SiO_2 interface under process conditions. The electron affinity of Ti(IV) in Ti–O–Si bonds is higher than in Ti–O–Ti bonds due to its electronic structure, expecting more electron injection. This is supported by the literature data of TiO_2/SiO_2 shown in Table 2. The SiO_2 on ZnO surface changes the surface charge due to the change in IEP of SiO_2, which prevents the formation of Zn^{2+}–dye aggregates on ZnO surface. From Table 2, Larger increase in J_{SC}, *i.e.* 7.66 mA/cm^2 has been observed for ZnO coated with SiO_2 (Table 2).

Presence of ZrO_2 as shell layer on TiO_2 at N3/TiO_2 has been observed not to change the values of J_{SC} and V_{OC} (in Table 2), due to its conduction band edge position. The E_{CB} (−3.41 eV) of ZrO_2 is higher than the LUMO level of the dye (−3.8 to 3.93 eV), so that the back electron injection cannot be prevented (Fig. 13). However, it can be seen that ZrO_2 has produced higher performance for the SnO_2/N719 interface-based DSSC. Hence upon revisiting and examining the data in Table 2, we have realized that larger difference in IEP value of core–shell materials has a role to play. It can be seen from Table 2 that core–shell materials with larger difference in the value of IEP has resulted with larger J_{SC}, suggesting the larger dipole moment play a major role in increasing the performance. The substantial increase in the η for metal oxide coated with Al_2O_3 and MgO layer have also suggested the same reason. The existence of larger dipole moment induces the excitons to diffuse into dye/metal oxide interface effectively where they undergo dissociation. Hence, the larger the dipole moment, the greater will be the dissociation. Doping or using shell material provide faster electron injection, in addition to lower recombination. Hence our examination on the performance of core–shell structure-based DSSC hints that the essential improvement in electron injection efficiency and thereby overall performance can be obtained by proper designing or choosing of the second metal oxide with suitable band gap, optimal thickness of shell layer and IEP.

6. Controlled electron transport by materials used in DSSCs

Electron injection from the dye introduces electron concentration in the metal oxide nanoparticulate matrix. It alters the energetics of the quasi-Fermi level of metal oxide and creates a potential gradient within particles, which is the driving force for electron transport. The efficiency of charge collection (η_c) is a function of charge transport and can be measured as follows:

$$\eta_c = 1 - \frac{R_t}{R_{rec}}$$

where R_t is the transport resistance and R_{rec} is the recombination resistance. For higher collection efficiency, the cell should render better transport of charges (low R_t) and with lesser recombination (low R_{rec}).

Metal oxide nanoparticles used in DSSCs are usually a random network of crystallographically misaligned crystallites [84] and as a consequence, lattice mismatches at the grain boundaries develops that could influence in electron scattering and act as electron trap (Fig. 13). For the nanoparticulate matrix with a thickness of 10 μm, approximately 10^6 grain boundaries are expected [26]. As a result, the electron transport will be limited and lead to electron accumulation in the nanoparticulate matrix. Accumulated electrons change the quasi-Fermi level and also undergo radiative energy losses, the electrons could either recombine with the electrolyte (back reaction) or the reduced dye.

6.1. Effect of 1D nanostructures for controlled electron transport

A grain boundary (GB) is the interface between two grains in a polycrystalline material. Grain boundaries disrupt the electron transport through a material and hence, grain boundaries in n-type metal oxide are considered as defects especially when they are

Table 2
Performance of core–shell nanostructures of metal oxides/dye in DSSC at AM 1.5.

Material		Band gap		IEP		Thickness or concentration of outer layer/dye	Performance values given in the bracket are the one that has been obtained without shell				Individual comments	Overall comments
Core	Shell	Core	Shell	Core	Shell		V_{OC} (V)	J_{SC} (mA/cm^2)	*FF*	η (%)		
TiO_2	$SrTiO_3$	3.3	3.2	6	8.6	N3 [70]	0.708 (0.650)	10.2 (10.5)	0.584 (0.536)	4 (3.81)	Larger increase in V_{OC}	Larger band gap shell materials increase the performance. MgO seems to be the better shell layer
TiO_2	MgO	3.3	7.2	6	12.7	N3 [108]	0.720 (0.640)	11.7 (0.64)	0.535 (0.473)	4.5 (3.1)	Largest increase in photocurrent	
TiO_2	ZrO_2	3.3	4.7	6	6.7	1:0.38/N3 [109]	–	–	–	2.27		
TiO_2	ZrO_2	3.3	4.7	6	6.7	N3 [110]	–	–	–	2.29 (1.36) at 0.1 sun	2-Fold increase in efficiency	
TiO_2	ZrO_2	3.3	4.7	6	6.7	N719 [76]	0.675 (0.735)	9.1 (9.1)	0.595 (0.551)	3.6 (3.7)	No significant change in photocurrent from N719	
TiO_2	SiO_2	3.3	8.9	6	2	0.53/Eosin [111]	0.600 (0.580)	0.55 (0.37)	0.54 (0.54)	0.18 (0.12)	Increase in V_{OC}	
TiO_2	SiO_2	3.3	8.9	6	2	N719 [76]	0.710 (0.735)	10.6 (9.1)	0.581 (0.551)	4.4 (3.7)	Larger photocurrent from N719 dye	
TiO_2	Al_2O_3	3.3	9.9	6	7–9	N719 [76]	0.760 (0.551)	12.1 (9.1)	0.611 (0.551)	5.6 (3.7)	Larger increase in photocurrent, V_{OC}, and *FF*. Thicker coating limits electron injection	
						4 times coated alumina/N719 [76]	0.860 (0.551)	2.45 (9.1)	0.656 (0.551)	1.4 (3.7)		
TiO_2	ZnO	3.3	3.3	6	9	30 nm thickness/N3 [75]	0.62 (0.49)	11.7 (13.2)	0.52 (0.40)	4.51 (3.31)	ZnO as the shell material increases V_{OC} and *FF*	
						60 nm thickness/N3 [75]	0.59 (0.49)	4.51 (13.2)	0.55 (0.40)	2.50 (3.31)	Lower recombination, but reduces the current	
						300 nm thickness/N3 [75]	0.47 (0.49)	0.61 (13.2)	0.51 (0.40)	0.18 (3.31)	Thickness of shell significantly reduces the current	
ZnO	TiO_2	3.3	3.3	9	6	TiO_2 with 10–25 nm thickness/N3 [71]	0.800	2.0	0.6 (0.36)	2.0 (0.85)	Increase in *FF*	SiO_2 is the better shell material
ZnO	SiO_2	3.3	8.9	9	2	1:5/N719 [60]	0.680 (0.670)	7.66 (1.0)	0.69 (0.73)	3.6 (0.52)	Larger increase in photocurrent	
SnO_2	ZrO_2	3.5	4.7	4	6.7	0.50/N719 [72]	0.550 (0.480)	12.9 (6.4)	0.47 (0.4)	3.4 (1.2)	Larger photocurrent	Significant increase in *FF* is observed for MgO coating
SnO_2	ZnO	3.5	3.3	4	9	0.59/N719 [72]	0.670 (0.480)	11.2 (6.4)	0.69 (0.4)	5.1 (1.2)	Larger photocurrent, V_{OC} and *FF*	
SnO_2	TiO_2	3.5	3.2	4	6	0.35/N719 [72]	0.660 (0.480)	10.9 (6.4)	0.54 (0.4)	3.9 (1.2)	Larger photocurrent, V_{OC} and *FF*	
SnO_2	MgO	3.5	7.2	4	12.7	0.13/N719	0.610 (0.480)	9.7 (6.4)	0.61 (0.4)	3.6 (1.2)	Increase in thickness reduces the *FF*, and V_{OC}, but increases the current	
						0.05/N719 [72]	0.800 (0.480)	7.0 (6.4)	0.72 (0.4)	4.0 (1.2)		
SnO_2	Al_2O_3	3.5	9.9	4	9	0.06/N719 [72]	0.740 (0.480)	10.0 (6.4)	0.70 (0.40)	5.2 (1.2)	Larger photocurrent	

intended to promote the electron conductivity. Electrons are trapped in these localized states, leaving a net negative charge at the GB. A band bending (V_B) will be formed in the vicinity of the GB preventing the diffusion of majority carriers towards the GB and attracting minority carriers into the GB, in turn, results in an increased level of electron-hole recombination in the GB region [85].

In one-dimensional (1D) nanostructures, the grain boundaries effect could be restricted (Fig. 15) [86,87]. Moreover, for the same given film thickness, the loading of dye can be much higher in 1D nanostructured material than the nanoparticles, for instance, the TiO_2 nanowires has allowed for larger adsorption of dye, *i.e.* 4 times than the P-25 [88]. The synthesis or preparation processes to obtain 1D nanostructured material have been demanding but time consuming. 1D nanostructures could act as single crystal, and involve in rapid electron transport. The formation of crystalline structure should depend on the methodology that is used for the preparation. The template assisted methodologies produce the 1D nanostructured materials with polycrystallinity in structure [89,90], which limit the electron transport, whereas the surfactant-controlled synthesis forms highly crystalline structure [89], an essential feature required for higher performance of DSSCs. Some of the commonly used methodologies and their significance with regards to the application in DSSCs are pointed out in Table 3.

In 1D nanostructures, the surface is focused and hence, the oxygen vacancy on the surface could be reduced and so act as better n-type material with good electronic transport property. The recombination rate has been found to be 10 times slower in 1D TiO_2 nanotubes which led for higher J_{SC} (7.8 mA/cm^2) than that of nanoparticles (2.6 mA/cm^2)-based DSSC [91]. Recently more effective charge transport has been realized when researchers attempted for direct deposition of rutile nanowires onto FTO conducting substrate [84]. However, the major problem of using 1D nanostructured electrodes in DSSCs, is their poor adhesion to substrates that arises due to the high temperature used for the sintering. During sintering, strong stresses are generated that lead to the shrinkage of the fibrous mats. Such shrinkage has limited the benefits of using 1D nanofibers film and resulting in poor charge collection. Hence, direct attachment (binding) of 1D nanostructured materials onto the conductive substrate (ITO or FTO) has

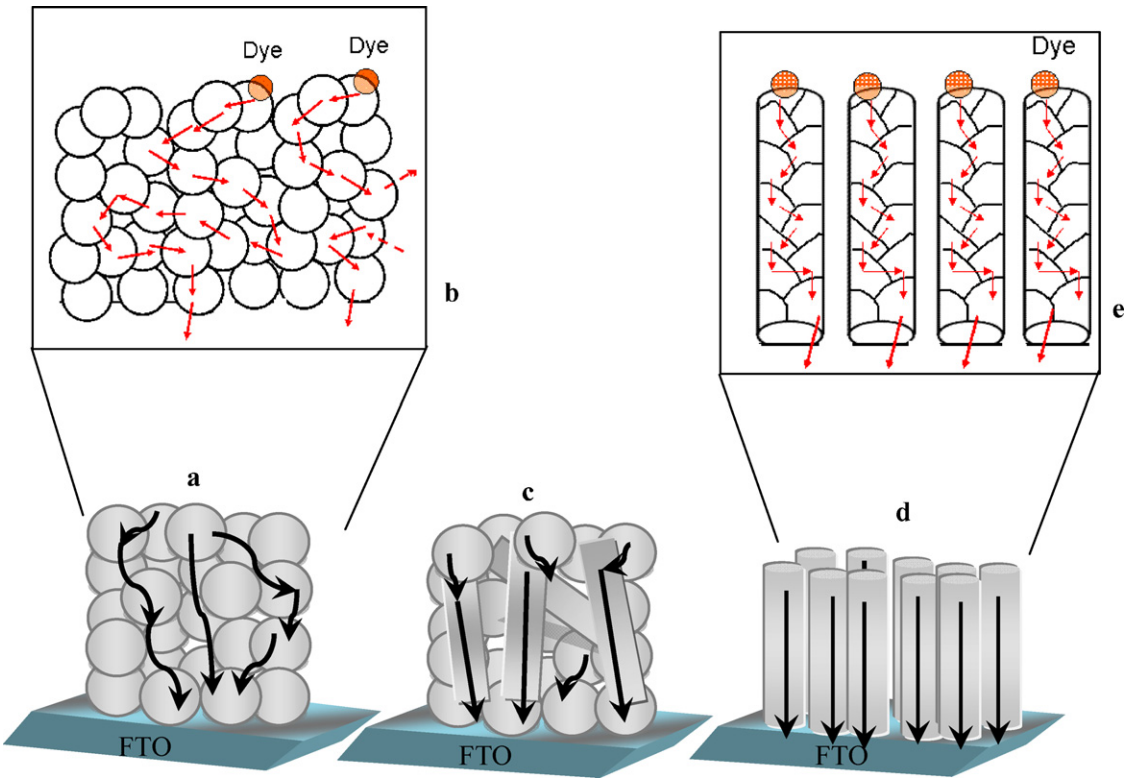

Fig. 13. (a) Electron scattering in metal oxide nanoparticles interface, (b) enlarged view of electron scattering in spherical nanoparticles interface, (c) reduced electron scattering in hybrid interface structure with particles and rods/wires and (d) more efficient electron transport possibility in vertically positioned 1D structures, (e) enlarged view of electron flow in 1D nanorods.

always been challenging. Song et al. [92] have used thin film of nanoparticles at the FTO as binding support for nanofibers on the FTO and also to prevent back electron transfer from ITO. Our group has successfully demonstrated direct deposition of electrospun TiO_2 nanofibers by introducing an ultra-thin surface treatment layer (STL) on the FTO before depositing the TiO_2 nanofibers. After calcination, the STL has behaved as an adhesive which retained adhesion of nanofibers on the conductive substrate and thus improved the adhesion of TiO_2 nanofibers for better electron transport [93].

6.2. Effect of hybrid nanostructure

Hybrid nanostructures (Fig. 13c) have recently emerged as a promising architecture for electron transport as well as dye adsorption. When the available quantity (and so the surface area) of spherical nanoparticles is larger in the hybrid structured photoanode film, especially towards the side that is disclosed for the dye adsorption in comparison with the 1D nanostructured materials, the maximum dye adsorption is possible on spherical particle surface, while the presence of nanofibers/rods, directs for faster electron transport rate (Table 4).

For hybrid matrix, the nanowires or rods that are used should preferably have the same crystal structure as nanoparticles for effective electron transport. Hybrid combination TiO_2 nanowires and P-25 with N719 dye has obtained an efficiency of 6.01% which is about 60% higher than that of DSSC based on TiO_2 nanowires alone [94]. As seen in Table 4, the hybrid of different morphological combination of TiO_2 has increased *FF* significantly compared to that of V_{OC}. This indicates hybrid structure improves the interpenetration of electrolyte in the hybrid matrix. The increase of V_{OC} of hybrid matrix of TiO_2 has been found little when compared to the single matrix (either P25 or nanofibers alone) and in some case, both are similar, suggesting the quasi Fermi energy

Table 3
A comparison of current methodology used for 1D nanostructures.

Nanostructure	Method	Advantages	Disadvantages
TiO_2 nanowires [112]	Phase transformation of gel matrix in shape container	Scattering of longer wavelength of light, good electron transport	Slow process for wire growth
TiO_2 nanotubes aligned [113]	Anodic oxidation of TiO_2 thin film	Higher efficiency up to 2.9%, excellent hollow structure	Low electrode thickness (360 nm), small working area
TiO_2 nanotubes random [114]	Surfactant assisted assemblies	Higher photocurrent, larger electron transport, single crystal, high BET surface	Slow process for nanotubes growth
TiO_2 nanotubes and nanorods [115]	Electrospinning and sol–gel	Good electron transport, industrial scalability, suitable solid electrolyte, high electrode thickness	Polycrystalline, poor adhesion of fibers onto FTO
ZnO nanowires [95]	Seed growth process in aqueous solution	Aspect ratio up to 125, higher electron transport, low temperature process.	Extremely slow process for wire growth
Dendrite ZnO nanowires [116]	Chemical vapor disposition	High electron transport, single crystal	Low surface area, low photocurrent, slow growth process

Table 4
Performance of hybrid materials/dye/liquid electrolyte[a] in DSSC.

Nanostructured acceptor		Donor	Cell area (cm^2)	Performance Values given in the bracket are the one that has been obtained only by using the material mentioned in "second combination" column				Comments
1D material	Second combination			V_{OC} (V)	J_{SC} (mA/cm^2)	*FF*	η (%)	
TiO_2 Nanorods 8.3 μm thick 10–20 nm diameter	TiO_2 P-25	N719 [117]	NA	0.73 (0.704)	13.97 (12.74)	0.70 (0.649)	7.12 (5.82)	Addition of nanorods increases electrolyte penetration, thus reduces recombination, results in larger J_{SC}, V_{OC}, and *FF*
TiO_2P-25	TiO_2 nanorods 15–18 μm thick 150 nm diameter	N3 [86]	1	0.834 (0.832)	13.3 (14.2)	O.477 (0.366)	5.26 (4.28)	Insertion of NP layer slightly decreases current, results in lower J_{SC}
TiO_2 nanowires 5.5 μm thick 5–30 nm diameter	TiO_2 P-25	N719 [94]	0.25	0.754 (0.714)	11.9 (8.16)	0.673 (0.710)	6.01 (4.13)	Addition of nanowires increases current generation, reduces recombination, results in larger J_{SC}, V_{OC}
TiO_2 nanowires 10–70 nm diameter 16 μm thick	TiO_2 NP	N719 [118]	NA	0.74 (0.74)	13.23 (12.11)	0.66 (0.63)	6.53 (5.59)	Increase in thickness increases the current
ZnO nanowires 5.5 μm thick 5–30 nm diameter	ZnO NP	Mercurochrome [99]	NA	0.61 (0.49)	6.3 (3.4)	0.58 (0.50)	2.2 (0.84)	Addition of ZnO nanowires significantly increases current, electrolyte penetration and so reduces recombination, results in larger J_{SC}, V_{OC}, and *FF*

[a] The electrolyte containing 1-hexy l-2,3-dimethyl-imidazolium iodide, I_2, LiI, 4-tert-butylpyridine, 3-methoxypropionitrile.

state of the TiO_2 is not affected by the hybrid composite. The hybrid of ZnO nanofibers and nanoparticles with mercurochrome dye has resulted with remarkable increase in the efficiency from 0.84% to 2.2%. Over all, J_{SC} of the hybrid composite has been found higher than the other efficiency parameters, which suggests hybrid structure increases the interfacial area that leads to more exciton dissociation and electron injection.

Although the 1D nanostructures have been proved to deliver higher J_{SC} than that of nanoparticles, the random aligned 1D matrix could be a barrier for the electrolyte interpenetration. 1D nanostructure TiO_2-based DSSCs with the standard liquid electrolyte have been found yielding relatively poor fill factor, *i.e.* in the range of 0.5–0.8 for the efficient dyes such as N3 and N719. This has raised the issue that the poor interpenetration is severe between 1D materials and the electrolyte. However, it is noted that lower *FF* has been compensated by the higher J_{SC}. Larger photocurrent could result from the possibility of more excitons generation due to large interface with dye and the controlled electron transport. Vertically aligned 1D metal oxides (Fig. 13d) in DSSCs can promote more exciton generation because of the possibility of larger binding of dye molecules. Furthermore, more dissociation can occur because of the formation of larger interfacial area, followed by more electron injection and transport compared to the non-aligned (random) 1D matrix. Law et al. [95] have developed vertical nanowires arrays of ZnO interface with N719 dye and observed that vertical nanowires facilitates faster electron injection than the ZnO nanoparticles/N719. However, the vertical nanowires-based device even with efficient dyes such as N3 and N719 have not yet yielded the considerable performance (refer Table 5). One of the possible reasons is the positioning of 1D nanomaterials. Closer spacing of nanofibers/wires increases the exciton dissociation and should be preferred in order to obtain larger J_{SC}. As known, the efficiency parameter *FF* is influenced by the metal oxide/electrolyte interface. Better the interpenetrating network between metal oxide and electrolyte, larger the *FF* and thus, higher the efficiency. Hence, the currently encountered poor fill factor (*FF*) issue in 1D architecture could also be improved in vertically nanostructured materials provided if they are positioned with its optimal height and space between nanowires. Methodologies to obtain such patterned nanostructures have been described well in the literatures [96,97]. Especially using electrospinning technique may be promising to control precisely both spacing and position as it can be automated and moreover, has the potential for large scale production [98].[1]

6.3. Effect of nanodimensions

With the advantages of having extremely high surface–volume aspect ratio and acting as a controlled unidirectional electron channel, the 1D nanostructures-based DSSC has been expected to deliver much higher conversion efficiency than the nanoparticles-based DSSC, however, it has not reached the best performance so far. Comparing the performance of nanofibers-based DSSCs in Table 4, it can be noted that the increase in the diameter of the fiber and thickness of the fiber matrix has resulted in an increase in V_{OC}, *FF* and J_{SC}. It can be realized that nanodimensions, *i.e.* diameter of 1D nanostructured metal oxide and the thickness of matrix used for electron transport play pivotal role. 1D nanostructures of larger thickness have been found to provide higher efficiency for TiO_2-based DSSCs. It is to be noted that the diffusion coefficient of electron is a function of diffusion length and residence time according to the correlation as follows:

$$L = \sqrt{D_e \tau_e}, \quad \text{where} D_e = kT\mu_e/e, i.e. L\alpha\tau_e \text{ and } L\alpha\mu_e$$

where L is the diffusion length, D_e is electron diffusion coefficient, τ_e is the residence time of electron and μ_e is electron mobility. Increase in diffusion length speeds up electron transport in nanoparticulate matrix by increasing the electronic mobility, simultaneously, it also increases the residence time of electron in

[1] Our group is currently focusing for controlled vertically patterned nanofibers with our industrial partners.

Table 5
Performance of DSSCs based on 1D structures of TiO2/dye/liquid electrolyte[a] at AM 1.5.

No.	Nanostructured TiO_2 acceptor	Donor	Cell area (cm^2)	Performance				Comments
				V_{OC} (V)	J_{SC} (mA/cm^2)	*FF*	η (%)	
1	Nanofibers 3.9 μm thick 20 nn diameter	N3 [119]	1	0.826	9.88	0.51	4.14	Nanorods reduces recombination, reflects as larger V_{OC} and J_{SC}
2	Nanofibers 20 μm thick 20 nm diameter	N3 [120]	0.16	0.77	11.24	0.58	5.02	Larger thickness leads to larger current
3	Nanorods 15–18 μm thick 500–600 nm long 150 nm diameter	N3 [86]	1.0	0.832	14.20	0.363	4.28	Longer length of nanorods increases the larger dye adsorption and thereby current to significantly larger (J_{SC})
4	Nanofibers 20 μm thick 20 nm diameter	N3 [96]	0.16	0.77	8.67	0.60	4.01	Larger thickness leads to larger current generation
5	Nanowires 7.9 μm thick 20–50 nm diameter	N719 [97]	NA	0.74	2.70	0.67	1.30	Smaller thickness leads to lower current generation
6	Nanowires (20%) 10 μm thick 20 nm long 5–10 nm diameter	N719 [88]	0.25	0.72	19.22	0.67	9.33	Hybrid structures increases the current and also electrolyte penetration
7	Nanofibers ~7 ± 3 μm thick 20 ± 8 nm diameter	N719 [121]	NA	0.59	4.21	0.60	1.50	Smaller thickness leads to lower current generation
8	Nanorods 13.7 μm thick 100–300 nm length 20–30 nm diameters	N719 [122]	0.25	0.767	13.10	0.728	7.29	Well defined aspect ratio of nanorods increases the current, improves electrolyte penetration and reduces recombination

[a] The electrolyte containing 1-hexyl-2,3-dimethyl-imidazolium iodide, I_2, LiI, 4-tert-butylpyridine, 3-methoxypropionitrile; the sintering temperature is 450–500 °C.

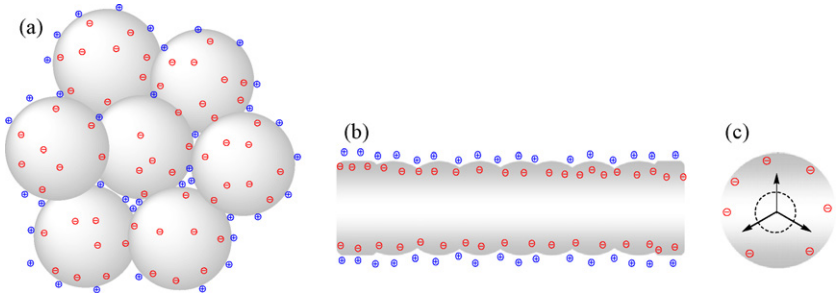

Fig. 14. Pictorial view to show the effect of shape influences the electron transport: (a) severe space charge layer discernible on spherical nanoparticles, (b) radical effect of 1D-nanofibers and (c) radical effect shown in the cross-sectional view of nanofibers.

the matrix. The hybrid mixture of nanoparticulate matrix film could increase the diffusion length for the same given thickness of nanoparticles matrix. For example, for the given film thickness of 5.5 μm, the hybrid composite of ZnO-nanowires/nanoparticles as nanoparticles matrix enhances the D_e, *i.e.* 2.1×10^{-4} cm^2 s^{-1} in comparison with the ZnO-nanoparticles alone as the matrix whose D_e is ~7.2×10^{-5} [99]. Increasing the thickness beyond optimal point will lead for longer electron residence time in metal oxide matrix that endangers the DSSC performance by easing the electron recombination with either the electrolyte or the reduced dye and also the energy state of metal oxide. High surface–volume ratio nature 1D nanostructure can accommodate more dye molecules while maintaining the confined thickness in DSSC and hence, materials recombination could be restricted. The electrolyte ions surround the nanoparticles (Fig. 14), thereby neutralize the electrostatic field whereas 1D structures such as nanofibers/nanorods with larger diameter can realize its cylindrical geometry that would create radial electric fields (Fig. 14), preventing the accumulation of more electrons, and thereby reducing chance for surface electron recombination.

It can be seen from Table 5 that nanorods morphology provides larger J_{SC} than that of nanofibers probably due to the well defined size-shape aspect ratio. Reduction in the diameter of the 1D nanostructures minimizes the grain interface effect as depicted in Fig. 15a and b, hence may result in higher efficiency. Concurrently, nanofibers with too larger diameter should be conducive to wider and uncontrolled electron scattering (Fig. 15b). This effect can be realized when comparing the dimensions of the fibers and their energy conversion performance shown in Table 5. Hence, researchers should realize the importance of the balance between diameter of the fibers and thickness of fiber matrix in 1D nanorods, nanofibers (nanowires) and impose for optimization.

The electron transport in ZnO nanorods interface with dye has been measured about 10–100 times faster than in nanoparticles [100,101]. The improvement in the crystalline nature of ceramic ZnO nanofibers could also reduce the formation of Zn^{2+}–dye aggregates. Recently, researchers have observed that ZnO nanorods renders rapid electron transport (<30 μs) [102]. Nevertheless, as shown in Table 6, the V_{OC} in the 1D nanostructured ZnO/dye/liquid electrolyte-based DSSCs have been poor although the electronic property of ZnO itself restricts the recombination behavior as mentioned earlier. Furthermore the electron life time (residence time) in the transport matrix could play an important role. For equally sized ZnO and TiO_2 nanoparticles, the electron lifetime has been found significantly longer in ZnO than in TiO_2. Researchers have measured τ_e as ~0.6 s for TiO_2 and 1 s for ZnO [103], under similar experimental conditions for the interfaces N719/TiO_2 and N719/ZnO. The electron residence (τ_e) in metal

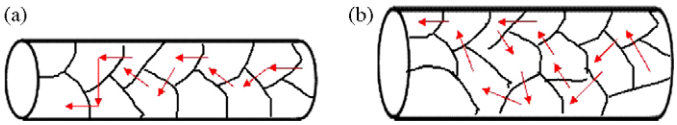

Fig. 15. Effect of diameter for controlling the electron transport: (a) less electron scattering in smaller diameter and (b) larger electron scattering in bigger diameter of nanorods.

Table 6
Performance of DSSCs based on 1D structures of ZnO/dye/liquid electrolyte[a] at AM 1.5.

No.	Nanostructured TiO_2 acceptor	Donor	Cell area (cm^2)	Performance				Comments
				V_{OC} (V)	J_{SC} (mA/cm^2)	*FF*	η (%)	
1	Vertical nanowires 5 μm thick 18–24 μm long 5–30 nm diameter	Mercurochrome [99]	NA	0.50	3.40	0.49	0.84	Vertical nanowires improves electron transport and thus shows higher current
2	Vertical nanowires 8 μm long 155 μm diameter	N719 [123]	NA	0.67	1.30	0.32	0.3	Bigger diameter (μm size) leads for poor penetration of electrolyte which reflects as lower *FF*
J	Vertical nanowire 25 μm thick 16–17 μm long 130–200 nm diameter	N719 [95]	0.2	0.71	5.85	0.38	1.5	Larger thickness of vertical nanowires leads to larger current generation. Higher V_{OC} is observed for these dimensions of nanowires
4	Nanorods 3.8 μm thick 3 μm long 200 nm diameter	N719 [101]	0.2	0.637	5.543	0.44	1.54	Well defined aspect ratio of nanorods increases the current, improves electrolyte penetration and reduces recombination

[a] The electrolyte containing 1-hexy l-2,3-dimethyl-imidazolium iodide, I2, LiI, 4-tert-butylpyridine, 3-methoxypropionitrile. The sintering temperature is 450–500 °C.

oxides is related to V_{OC} as such, τ_e increases with decrease in V_{OC} as per the correlation [104]:

$$\tau_e = -\frac{kT}{e}\left(\frac{dV_{OC}}{dt}\right)^{-1}$$

where k is the Boltzmann constant, T is the absolute temperature, and e is the elementary charge. Hence increasing the thickness of 1D ZnO nanomaterials-based film could facilitate for larger recombination with the electrolyte when it exceeds the optimal thickness. The optimal thickness has to be designed based on the spectral range of dye and the type of metal oxide employed in DSSC.

This review has not covered other important factors such as effect of pore size of materials, sintering temperature, and electrolytes etc though they influence electron injection and transport significantly. There are other excellent reviews which have covered such factors and are available elsewhere [12,105–107].

7. Conclusion and future directions

For DSSC to have a real impact in the commercial domain, mastering the factors that control the electron injection and transport at the materials interfaces is vital. The development of new dye materials, transport materials, electrolytes, hole transport materials has countenanced interfaces to be formed efficiently and in many cases elegantly. The electrons are injected across the dye/metal oxide interface into metal oxide, a process that is controlled by the energetics between dye and metal oxide, electronic states and chemical nature of metal oxides, and process condition. Although we have not given any direct correlation between chemical property of the metal oxides and device performance in this review, we confide that the properties such as IEP are also critical factor in designing the interface. 1D nanomorphologies render controlled (surface focused) unidirectional electron pathway in the metal oxides, however, the performance of 1D-based DSSCs has not been the best yet despite the endowment of larger dye loading and rapid electron transport. This review has identified diameter of 1D nanomaterials and thickness of film are dominant factors that control the electron transport. It will be particularly important to use both theory and experiment to explore in-depth and reveal all the factors that are barriers for 1D nanostructured materials and their interfaces with dye and electrolyte from sterling performance. Larger area of interface is necessary for more exciton separation, which could be achieved in 1D nanorods (fibers) and wires even for a limited film thickness nonetheless we cannot rule out the possibility that increasing the interface area to a certain extent could also lead to high interfacial recombination. Thus for ESC especially DSSCs, researchers have to carefully form the interface with right combination of donor and acceptor materials, and control the interface to yield complete dissociation of electron and hole under optimized operating condition. DSSCs nowadays pay attention, not only to obtain higher solar-current conversion efficiency, and also by their potential for being cost-effective, and more stable for longer period of time. Caution must be exercised when more materials are involved in DSSCs as there will be trouble for scaling up the cell design and controlling the manufacturing the cost. Researchers therefore currently concentrate on maximizing the performance of DSSCs by developing multifunctional engineered materials-based interfaces as well as reducing the complexity in the cell design to make DSSCs entirely a commercially viable.

Acknowledgements

VT and SR would like to express thanks to NUS President's office special program grant. VR also expresses his thanks to Harvard Medical School. Authors also acknowledge Mr. A. Kumar for providing his master degree thesis for reference. VT also acknowledges to Dr. G. Balaji for his technical comments to improve this manuscript.

References

[1] M.A. Green, K. Emery, Y. Hisikawa, W. Warta, Prog. Photovoltaics 15 (2007) 425–430.
[2] B. O'Regan, M. Graetzel, Nature 353 (1991) 737–740.
[3] Y. Kim, S. Cook, S.M. Tuladhar, S.A. Choulis, J. Nelson, J.R. Durrant, D.D.C. Bradley, M. Giles, I. McCulloch, C.-S. Ha, M. Ree, Nature Mater. 5 (2006) 197–203.
[4] W.U. Huynh, J.J. Dittmer, A.P. Alivisatos, Science 295 (2002) 2425–2427.
[5] N. Robertson, Angew. Chem. Int. Ed. 45 (2006) 2338–2345.
[6] H. Tian, F. Meng, Opt. Sci. Eng. 99 (2005) 313–329.
[7] M. Gratzel, Prog. Photovoltaics 14 (2006) 429–442.
[8] M.A. Green, Mater. Energy Convers. Dev. (2005) 3–34.
[9] S.E. Gledhill, B. Scott, B.A. Gregg, J. Mater. Res. 20 (2005) 3167–3179.
[10] M. Gorlov, L. Kloo, Dalton Trans. (2008) 2655–2666.
[11] O.V. Chervakov, M.V. Burmistr, O.S. Sverdlikovs'ka, V.H. Shapka, Polimernii Zhurnal 30 (2008) 5–13.
[12] H.J. Snaith, L. Schmidt-Mende, Adv. Mater. 19 (2007) 3187–3200.
[13] N. Kopidakis, K.D. Benkstein, J. Van de Lagemaat, A.J. Frank, J. Phys. Chem. B 107 (2003) 11307–11315.
[14] J. Bisquert, Phys. Chem. Chem. Phys. 10 (2008) 3175–3194.
[15] J. Bisquert, A. Zaban, M. Greenshtein, I. Mora-Sero, J. Am. Chem. Soc. 126 (2004) 13550–13559.

[16] A. Kambili, A.B. Walker, F.L. Qiu, A.C. Fisher, A.D. Savin, L.M. Peter, Physica E 14 (2002) 203–209.
[17] N. Papageorgiou, M. Graetzel, P.P. Infelta, Sol. Energy Mater. Sol. Cells 44 (1996) 405–438.
[18] A. Solbrand, H. Lindstroem, H. Rensmo, A. Hagfeldt, S.-E. Lindquist, S. Soedergren, J. Phys. Chem. B 101 (1997) 2514–2518.
[19] F. Cao, G. Oskam, P.C. Searson, J. Phys. Chem. 100 (1996) 17021–17027.
[20] T. Dittrich, Phys. Status Solidi A: Appl. Res. 182 (2000) 447–455.
[21] A. Solbrand, A. Henningsson, S. Soedergren, H. Lindstroem, A. Hagfeldt, S.-E. Lindquist, J. Phys. Chem. B 103 (1999) 1078–1083.
[22] M. Yanagida, K. Miyamoto, K. Sayama, K. Kasuga, M. Kurashige, Y. Abe, H. Sugihara, J. Phys. Chem. C 111 (2007) 201–209.
[23] A.N.M. Green, E. Palomares, S.A. Haque, J.M. Kroon, J.R. Durrant, J. Phys. Chem. B 109 (2005) 12525–12533.
[24] H. Usui, H. Matsui, N. Tanabe, S. Yanagida, J. Photochem. Photobiol. A: Chem. 164 (2004) 97–101.
[25] B.A. Gregg, M.C. Hanna, J. Appl. Phys. 93 (2003) 3605–3614.
[26] L. Hu, S. Dai, J. Weng, S. Xiao, Y. Sui, Y. Huang, S. Chen, F. Kong, X. Pan, L. Liang, K. Wang, J. Phys. Chem. B 111 (2007) 358–362.
[27] S.E. Shaheen, C.J. Brabec, N.S. Sariciftci, F. Padinger, T. Fromherz, J.C. Hummelen, Appl. Phys. Lett. 78 (2001) 841–843.
[28] C.J. Brabec, A. Cravino, D. Meissner, N.S. Sariciftci, T. Fromherz, M.T. Rispens, L. Sanchez, J.C. Hummelen, Adv. Funct. Mater. 11 (2001) 374–380.
[29] G.W. Crabtree, N.S. Lewis, Phys. Today 60 (2007) 37–42.
[30] M.K. Nazeeruddin, P. Pechy, T. Renouard, S.M. Zakeeruddin, R. Humphry-Baker, P. Comte, P. Liska, L. Cevey, E. Costa, V. Shklover, L. Spiccia, G.B. Deacon, C.A. Bignozzi, M. Graetzel, J. Am. Chem. Soc. 123 (2001) 1613–1624.
[31] M. Nilsing, P. Persson, S. Lunell, L. Ojamaee, J. Phys. Chem. C 111 (2007) 12116–12123.
[32] J. Rochford, D. Chu, A. Hagfeldt, E. Galoppini, J. Am. Chem. Soc. 129 (2007) 4655–4665.
[33] R. Jose, A. Kumar, V. Thavasi, K. Fujihara, S. Uchida, S. Ramakrishna, Appl. Phys. Lett. 93 (2008) 023125/023121–023125/023123.
[34] R. Jose, A. Kumar, V. Thavasi, S. Ramakrishna, Nanotechnology 19 (2008) 424004.
[35] E. Bae, W. Choi, J. Park, H.S. Shin, S.B. Kim, J.S. Lee, J. Phys. Chem. B 108 (2004) 14093–14101.
[36] M. Nilsing, P. Persson, L. Ojamaee, Chem. Phys. Lett. 415 (2005) 375–380.
[37] H. Park, E. Bae, J.-J. Lee, J. Park, W. Choi, J. Phys. Chem. B 110 (2006) 8740–8749.
[38] A. Vittadini, A. Selloni, F.P. Rotzinger, M. Graetzel, J. Phys. Chem. B 104 (2000) 1300–1306.
[39] K.S. Finnie, J.R. Bartlett, J.L. Woolfrey, Langmuir 14 (1998) 2744–2749.
[40] M.K. Nazeeruddin, R. Humphry-Baker, P. Liska, M. Graetzel, J. Phys. Chem. B 107 (2003) 8981–8987.
[41] C. Bauer, G. Boschloo, E. Mukhtar, A. Hagfeldt, J. Phys. Chem. B 106 (2002) 12693–12704.
[42] K. Murakoshi, G. Kano, Y. Wada, S. Yanagida, H. Miyazaki, M. Matsumoto, S. Murasawa, J. Electroanal. Chem. 396 (1995) 27–34.
[43] V. Shklover, Y.E. Ovchinnikov, L.S. Braginsky, S.M. Zakeeruddin, M. Graetzel, Chem. Mater. 10 (1998) 2533–2541.
[44] A. Furube, M. Murai, S. Watanabe, K. Hara, R. Katoh, M. Tachiya, J. Photochem. Photobiol. A: Chem. 182 (2006) 273–279.
[45] P. Wang, S.M. Zakeeruddin, P. Comte, R. Charvet, R. Humphry-Baker, M. Graetzel, J. Phys. Chem. B 107 (2003) 14336–14341.
[46] B. Wenger, M. Gratzel, E. Moser Jacques, J. Am. Chem. Soc. 127 (2005) 12150–12151.
[47] M. Graetzel, Inorg. Chem. 44 (2005) 6841–6851.
[48] D.P. Hagberg, T. Marinado, K.M. Karlsson, K. Nonomura, P. Qin, G. Boschloo, T. Brinck, A. Hagfeldt, L. Sun, J. Org. Chem. 72 (2007) 9550–9556.
[49] J. Guo, D. Stockwell, X. Ai, C. She, N.A. Anderson, T. Lian, J. Phys. Chem. B 110 (2006) 5238–5244.
[50] J. Guo, C. She, T. Lian, J. Phys. Chem. C 111 (2007) 8979–8987.
[51] J.B. Asbury, E. Hao, Y. Wang, H.N. Ghosh, T. Lian, J. Phys. Chem. B 105 (2001) 4545–4557.
[52] S. Iwai, K. Hara, S. Murata, R. Katoh, H. Sugihara, H. Arakawa, J. Chem. Phys. 113 (2000) 3366–3373.
[53] C. Bauer, G. Boschloo, E. Mukhtar, A. Hagfeldt, Int. J. Photoenergy 4 (2002) 17–20.
[54] G. Benko, P. Myllyperkio, J. Pan, P. Yartsev Arkady, V. Sundstrom, J. Am. Chem. Soc. 125 (2003) 1118–1119.
[55] W. Li, A.I. Frenkel, J.C. Woicik, C. Ni, S.I. Shah, Phys. Rev. B: Conden. Matter Mater. Phys. 72 (2005) 155315/155311–155315/155316.
[56] K. Keis, E. Magnusson, H. Lindstrom, S.-E. Lindquist, A. Hagfeldt, Sol. Energy Mater. Sol. Cells 73 (2002) 51–58.
[57] K. Kakiuchi, E. Hosono, S. Fujihara, J. Photochem. Photobiol. A: Chem. 179 (2006) 81–86.
[58] X. Ai, N.A. Anderson, J. Guo, T. Lian, J. Phys. Chem. B 109 (2005) 7088–7094.
[59] X. Ai, J. Guo, N.A. Anderson, T. Lian, J. Phys. Chem. B 108 (2004) 12795–12803.
[60] H. Tributsch, Coord. Chem. Rev. 248 (2004) 1511–1530.
[61] H. Tributsch, Appl. Phys. A: Mater. Sci. Process 73 (2001) 305–316.
[62] H. Horiuchi, R. Katoh, K. Hara, M. Yanagida, S. Murata, H. Arakawa, M. Tachiya, J. Phys. Chem. B 107 (2003) 2570–2574.
[63] K. Keis, J. Lindgren, S.-E. Lindquist, A. Hagfeldt, Langmuir 16 (2000) 4688–4694.
[64] N.A. Anderson, X. Ai, T. Lian, J. Phys. Chem. B 107 (2003) 14414–14421.
[65] K. Hara, T. Horiguchi, T. Kinoshita, K. Sayama, H. Sugihara, H. Arakawa, Chem. Lett. (2000) 316–317.
[66] C.-Y. Chen, S.-J. Wu, C.-G. Wu, J.-G. Chen, K.-C. Ho, Angew. Chem. Int. Ed. 45 (2006) 5822–5825.
[67] M.K. Nazeeruddin, P. Pechy, M. Graetzel, Chem. Commun. (1997) 1705–1706.
[68] J.A. Pollard, D. Zhang, J.A. Downing, F.J. Knorr, J.L. McHale, J. Phys. Chem. A 109 (2005) 11443–11452.
[69] D.F. Watson, G.J. Meyer, Coord. Chem. Rev. 248 (2004) 1391–1406.
[70] Y. Diamant, S.G. Chen, O. Melamed, A. Zaban, J. Phys. Chem. B 107 (2003) 1977–1981.
[71] P. Balaya, J. Jamnik, J. Fleig, J. Maier, J. Electrochem. Soc. 154 (2007) P69–P76.
[72] E. Kroeze Jessica, N. Hirata, S. Koops, K. Nazeeruddin Md, L. Schmidt-Mende, M. Gratzel, R. Durrant James, J. Am. Chem. Soc. 128 (2006) 16376–16383.
[73] A. Haque Saif, E. Palomares, M. Cho Byung, N.M. Green Alex, N. Hirata, R. Klug David, R. Durrant James, J. Am. Chem. Soc. 127 (2005) 3456–3462.
[74] A. Staniszewski, G.J. Meyer, PMSE Preprints 95 (2006) 294.
[75] S.-J. Roh, R.S. Mane, S.-K. Min, W.-J. Lee, C.D. Lokhande, S.-H. Han, Appl. Phys. Lett. 89 (2006) 253512/253511–253512/253513.
[76] E. Palomares, J.N. Clifford, S.A. Haque, T. Lutz, J.R. Durrant, J. Am. Chem. Soc. 125 (2003) 475–482.
[77] Y.-J. Shin, J.-H. Lee, J.-H. Park, N.-G. Park, Chem. Lett. 36 (2007) 1506–1507.
[78] C.M. Martin, V.M. Burlakov, H.E. Assender, Sol. Energy Mater. Sol. Cells 90 (2006) 900–915.
[79] J.-A. He, R. Mosurkal, J. Kumar, L. Li, K.G. Chittibabu, L.A. Samuelson, Mater. Res. Soc. Symp. Proc. 710 (2002) 213–218.
[80] E. Palomares, A. Green, S.A. Haque, J.R. Durrant, Proc. SPIE-Int. Soc. Opt. Eng. 5520 (2004) 76–81.
[81] F. Lenzmann, M. Nanu, O. Kijatkina, A. Belaidi, Thin Solid Films 451–452 (2004) 639–643.
[82] S.A. Haque, E. Palomares, C. Xu, R.J. Potter, A.B. Holmes, J.R. Durrant, Proc. SPIE-Int. Soc. Opt. Eng. 5215 (2004) 9–15.
[83] F. Fabregat-Santiago, J. Garcia-Canadas, E. Palomares, J.N. Clifford, S.A. Haque, J.R. Durrant, G. Garcia-Belmonte, J. Bisquert, J. Appl. Phys. 96 (2004) 6903–6907.
[84] T. Berger, T. Lana-Villarreal, D. Monllor-Satoca, R. Gomez, J. Phys. Chem. C 111 (2007) 9936–9942.
[85] A.C. Bose, P. Balaya, P. Thangadurai, S. Ramasamy, J. Phys. Chem. Solids 64 (2003) 659–663.
[86] K. Fujihara, A. Kumar, R. Jose, S. Ramakrishna, S. Uchida, Nanotechnology 18 (2007) 365709/365701–365709/365705.
[87] J.B. Baxter, E.S. Aydil, Sol. Energy Mater. Sol. Cells 90 (2006) 607–622.
[88] M. Adachi, Y. Murata, J. Takao, J. Jiu, M. Sakamoto, F. Wang, J. Am. Chem. Soc. 126 (2004) 14943–14949.
[89] Y. Xia, P. Yang, Y. Sun, Y. Wu, B. Mayers, B. Gates, Y. Yin, F. Kim, H. Yan, Adv. Mater. 15 (2003) 353–389.
[90] J.G. Lu, P. Chang, Z. Fan, Mater. Sci. Eng. R: Reports R52 (2006) 49–91.
[91] K. Zhu, N.R. Neale, A. Miedaner, A.J. Frank, NanoLetters 7 (2007) 69–74.
[92] M.Y. Song, Y.R. Ahn, S.M. Jo, D.Y. Kim, Mater. Res. Soc. Symp. Proc. 836 (2005) 107–112.
[93] R. Zhu, C.-Y. Jiang, X.-Z. Liu, B. Liu, A. Kumar, S. Ramakrishna, Appl. Phys. Lett. 93 (2008) 013102/013101–013102/013103.
[94] Y. Suzuki, S. Ngamsinlapasathian, R. Yoshida, S. Yoshikawa, Central Eur. J. Chem. 4 (2006) 476–488.
[95] M. Law, L.E. Greene, J.C. Johnson, R. Saykally, P. Yang, Nature Mater. 4 (2005) 455–459.
[96] T. Kuykendall, P.J. Pauzauskie, Y. Zhang, J. Goldberger, D. Sirbuly, J. Denlinger, P. Yang, Nature Mater. 3 (2004) 524–528.
[97] G.T. Wang, A.A. Talin, D.J. Werder, J.R. Creighton, E. Lai, R.J. Anderson, I. Arslan, Nanotechnology 17 (2006) 5773–5780.
[98] V. Thavasi, G. Singh, S. Ramakrishna, Energy Environ. Sci. 1 (2008) 205, doi:10.1039/b809074m.
[99] C.-H. Ku, J.-J. Wu, Appl. Phys. Lett. 91 (2007) 093117/093111–093117/093113.
[100] A.B.F. Martinson, J.E. McGarrah, M.O.K. Parpia, J.T. Hupp, Phys. Chem. Chem. Phys. 8 (2006) 4655–4659.
[101] K.S. Kim, Y.-S. Kang, J.-H. Lee, Y.-J. Shin, N.-G. Park, K.S. Ryu, S.H. Chang, Bull. Korean Chem. Soc. 27 (2006) 295–298.
[102] E. Galoppini, J. Rochford, H. Chen, G. Saraf, Y. Lu, A. Hagfeldt, G. Boschloo, J. Phys. Chem. B 110 (2006) 16159–16161.
[103] M. Quintana, T. Edvinsson, A. Hagfeldt, G. Boschloo, J. Phys. Chem. C 111 (2007) 1035–1041.
[104] A. Zaban, M. Greenshtein, J. Bisquert, Chem. Phys. Chem. 4 (2003) 859–864.
[105] S. Fujihara, K. Kakiuchi, E. Hosono, Electrochemistry (2005) 133–157.
[106] A. Zaban, Nanocryst. Metals Oxides (2002) 209–234.
[107] C. Longo, M.-A. De Paoli, J. Braz. Chem. Soc. 14 (2003) 889–901.
[108] H.S. Jung, J.-K. Lee, M. Nastasi, S.-W. Lee, J.-Y. Kim, J.-S. Park, K.S. Hong, H. Shin, Langmuir 21 (2005) 10332–10335.
[109] D.B. Menzies, R. Cervini, Y.-B. Cheng, G.P. Simon, L. Spiccia, J. Sol–Gel Sci. Technol. 32 (2004) 363–366.
[110] D. Menzies, Q. Dai, Y.B. Cheng, G.P. Simon, L. Spiccia, Mater. Lett. 59 (2005) 1893–1896.
[111] T.-V. Nguyen, H.-C. Lee, M.A. Khan, O.B. Yang, Sol. Energy 81 (2007) 529–534.
[112] M. Duerr, A. Schmid, M. Obermaier, S. Rosselli, A. Yasuda, G. Nelles, Nature Mater. 4 (2005) 607–611.
[113] G.K. Mor, K. Shankar, M. Paulose, O.K. Varghese, C.A. Grimes, NanoLetters 6 (2006) 215–218.

[114] M. Adachi, Y. Murata, I. Okada, S. Yoshikawa, J. Electrochem. Soc. 150 (2003) G488–G493.
[115] M.Y. Song, Y.R. Ahn, S.M. Jo, D.Y. Kim, J.-P. Ahn, Appl. Phys. Lett. 87 (2005), 113113/113111–113113/113113.
[116] J.B. Baxter, E.S. Aydil, Appl. Phys. Lett. 86 (2005), 053114/053111–053114/053113.
[117] S. Pavasupree, S. Ngamsinlapasathian, M. Nakajima, Y. Suzuki, S. Yoshikawa, J Photochem. Photobiol. A Chem. 184 (2006) 163–169.
[118] K. Asagoe, Y. Suzuki, S. Ngamsinlapasathian, S. Yoshikawa, J. Phys. Conference Series 61 (2007) 1112–1116.
[119] K. Onozuka, B. Ding, Y. Tsuge, T. Naka, M. Yamazaki, S. Sugi, S. Ohno, M. Yoshikawa, S. Shiratori, Nanotechnology 17 (2006) 1026–1031.
[120] M.Y. Song, D.K. Kim, K.J. Ihn, S.M. Jo, D.Y. Kim, Nanotechnology 15 (2004) 1861–1865.
[121] E. Enache-Pommer, J.E. Boercker, E.S. Aydil, Appl. Phys. Lett. 91 (2007), 123116/123111–123116/123113.
[122] J. Jiu, S. Isoda, F. Wang, M. Adachi, J. Phys. Chem. B 110 (2006) 2087–2092.
[123] J.B. Baxter, A.M. Walker, K. van Ommering, E.S. Aydil, Nanotechnology 17 (2006) S304–S312.